

**Modeling Half-Cell Potentials and their Relationship to Corrosion of  
Reinforcing Steel**

BY

Justin Milne Wilson

B.S. Univeristy of Massachusetts Lowell (2012)

SUBMITTED IN PARTIAL FULFILLMENT OF THE REQUIREMENTS FOR  
THE DEGREE OF MASTER OF SCIENCE  
DEPARTMENT OF CIVIL AND ENVIRONEMNTAL ENGINEERING  
UNIVERSITY OF MASSACHUSETTS LOWELL

**Signature of Author:** \_\_\_\_\_ **Date:** \_\_\_\_\_

Department of Civil and Environmental Engineering  
May 2013

**Signature of Thesis Supervisor:** \_\_\_\_\_

Tzu-Yang Yu  
Assistant Professor

**Committee Member Signature:** \_\_\_\_\_

Professor Donald Leitch  
Department of Civil and Environmental Engineering

**Committee Member Signature:** \_\_\_\_\_

Professor Susan Faraji  
Department of Civil and Environmental Engineering

**Modeling Half-Cell Potentials and their Relationship to Corrosion of  
Reinforcing Steel**

BY

Justin Milne Wilson

B.S. Univeristy of Massachusetts Lowell (2012)

ABSTRACT OF A THESIS SUBMITTED TO THE FACULTY OF THE  
DEPARTMENT OF CIVIL AND ENVIRONMENTAL ENGINEERING  
IN PARTIAL FULFILLMENT OF THE REQUIREMENTS  
FOR THE DEGREE OF  
MASTER OF SCIENCE  
UNIVERSITY OF MASSACHUSETTS LOWELL  
2013

Thesis Supervisor: Tzu-Yang Yu, Ph.D.  
Associate Professor, Department of Civil and Environmental Engineering

# Abstract

Monitoring of corrosion is one of the greatest challenges facing civil engineers today. All structures require monitoring to ensure they can operate safely under service loads. Reinforced concrete structures need a special kind of monitoring because corrosion can severely damage the structure and cause failure. Many types of testing exist such as destructive testing and ultrasonic testing. The half-cell potential method offers a standardized way to test for the level of corrosion without destroying the specimen. An adapted version of the modified Southern Exposure Test was performed and reasonable results were obtained with the half-cell potential method. The time history of the measurements was plotted, effect of spatail location and concrete cover proved, and the current density was calculated and plotted for each week of the experiment.

# Acknowledgements

I would like to thank my advisor, Dr. Tzu-Yang Yu for his guidance throughout my tenure and help in compiling this thesis. I would also like to thank professors Donald Leitch and Susan Faraji for sitting on my thesis committee. I would also like to thank the UMass Lowell Concrete Canoe team for giving me plenty of distractions when I needed them. I would also like to thank Suppa's Subs and Pizza for providing cheap food for all those long nights. Last but not least, I would like to thank my family for their support throughout this grueling process.

# Contents

<b>1</b>	<b>Introduction</b>	<b>1</b>
1.1	Research Objective . . . . .	4
1.2	Thesis Approach . . . . .	4
1.3	Organization of the Thesis . . . . .	5
<b>2</b>	<b>Literature Review</b>	<b>6</b>
2.1	Half-Cell Potential . . . . .	7
2.2	Current Density . . . . .	17
2.3	Summary . . . . .	20
<b>3</b>	<b>Experimental Method</b>	<b>21</b>
3.1	Half-Cell Potential Voltmeter . . . . .	21
3.2	The Slabs . . . . .	23
3.3	Test Procedure . . . . .	24
3.4	Summary . . . . .	25
<b>4</b>	<b>Experimental Results</b>	<b>26</b>
4.1	Time-Dependent Half-Cell Potentials . . . . .	27
4.1.1	Slab 1 . . . . .	27
4.1.2	Slab 2 . . . . .	33

4.1.3	Slab 3 . . . . .	39
4.1.4	Slab 4 . . . . .	42
4.2	Current Density . . . . .	49
4.2.1	Slab 1 . . . . .	49
4.2.2	Slab 2 . . . . .	50
4.2.3	Slab 3 . . . . .	53
4.2.4	Slab 4 . . . . .	59
4.3	Summary . . . . .	62
<b>5</b>	<b>Conclusions</b>	<b>63</b>
5.1	Research Findings . . . . .	64
5.2	Contributions . . . . .	65
5.3	Future Work . . . . .	65

# List of Figures

1.1	Schematic of HCP Test Method . . . . .	3
1.2	Layout of Steel Reinforcement . . . . .	5
3.1	Half-Cell Sensor . . . . .	22
3.2	Methodology of the Thesis . . . . .	25
4.1	Contour Map of Slab 1 on 23 March 2012, Week 11 . . . . .	28
4.2	Contour Map of Slab 1 on 25 May 2012, Week 20 . . . . .	28
4.3	Contour Map of Slab 1 on 10 October 2012, Week 40 . . . . .	29
4.4	Contour Map of Slab 1 on 4 January 2013, Week 52 . . . . .	29
4.5	Minimum, Average, and Maximum HCP as of Week 52 . . . . .	30
4.6	Minimum HCP Data and Cubic Polynomial as of Week 52 . . . . .	31
4.7	Average HCP Data and Cubic Polynomial as of Week 52 . . . . .	32
4.8	Contour Map of Slab 2 on 23 March 2012, Week 11 . . . . .	33
4.9	Contour Map of Slab 2 on 25 May 2012, Week 20 . . . . .	34
4.10	Contour Map of Slab 2 on 10 October 2012, Week 40 . . . . .	34
4.11	Contour Map of Slab 2 on 4 January 2013, Week 52 . . . . .	35
4.12	Minimum, Average, and Maximum HCP as of Week 52 . . . . .	36
4.13	Minimum HCP Data and Cubic Polynomial as of Week 52 . . . . .	37
4.14	Average HCP Data and Cubic Polynomial as of Week 52 . . . . .	38

4.15	Contour Map of Slab 3 on 23 March 2012, Week 11 . . . . .	39
4.16	Contour Map of Slab 3 on 25 May 2012, Week 20 . . . . .	40
4.17	Contour Map of Slab 3 on 10 October 2012, Week 40 . . . . .	40
4.18	Contour Map of Slab 3 on 4 January 2013, Week 52 . . . . .	41
4.19	Minimum, Average, and Maximum HCP as of Week 52 . . . . .	42
4.20	Minimum HCP Data and Cubic Polynomial as of Week 52 . . . . .	43
4.21	Average HCP Data and Cubic Polynomial as of Week 52 . . . . .	43
4.22	Contour Map of Slab 4 on 23 March 2012, Week 11 . . . . .	44
4.23	Contour Map of Slab 4 on 25 May 2012, Week 20 . . . . .	45
4.24	Contour Map of Slab 4 on 10 October 2012, Week 40 . . . . .	45
4.25	Contour Map of Slab 4 on 4 January 2013, Week 52 . . . . .	46
4.26	Minimum, Average, and Maximum HCP as of Week 52 . . . . .	46
4.27	Minimum HCP Data and Cubic Polynomial as of Week 52 . . . . .	47
4.28	Average HCP Data and Cubic Polynomial as of Week 52 . . . . .	48
4.29	Current Density of Slab 1, Bars 1 and 2 . . . . .	50
4.30	Current Density of Slab 1, Bars 3 and 4 . . . . .	51
4.31	Current Density of Slab 1, Bars 5 and 6 . . . . .	51
4.32	Current Density of Slab 1, Bars 7 and 8 . . . . .	52
4.33	Current Density of Slab 2, Bars 1 and 2 . . . . .	53
4.34	Current Density of Slab 2, Bars 3 and 4 . . . . .	54
4.35	Current Density of Slab 2, Bars 5 and 6 . . . . .	54
4.36	Current Density of Slab 2, Bars 7 and 8 . . . . .	55
4.37	Current Density of Slab 3, Bars 1 - 4 . . . . .	56
4.38	Current Density of Slab 3, Bars 5 - 8 . . . . .	57
4.39	Current Density of Slab 3, Bars 9 - 11 . . . . .	57

4.40 Current Density of Slab 3, Bars 12 - 14 . . . . . 58  
4.41 Current Density of Slab 4, Bars 1 - 4 . . . . . 59  
4.42 Current Density of Slab 4, Bars 5 - 8 . . . . . 60  
4.43 Current Density of Slab 4, Bars 9 - 11 . . . . . 60  
4.44 Current Density of Slab 4, Bars 12 - 14 . . . . . 61

# List of Tables

4.1	Parameters for Slab 1 . . . . .	31
4.2	Parameters for Slab 2 . . . . .	36
4.3	Parameters for Slab 3 . . . . .	42
4.4	Parameters for Slab 4 . . . . .	47
4.5	Current Densities and Changes for Slab 1 . . . . .	52
4.6	Current Densities and Changes for Slab 2 . . . . .	55
4.7	Current Densities and Changes for Slab 3 . . . . .	58
4.8	Current Densities and Changes for Slab 4 . . . . .	61

# Chapter 1

## Introduction

Concrete has been used in various forms since ancient Roman times. Some of the world's most spectacular structures, such as the Pantheon, are made solely of concrete. Many of these ancient monuments are unreinforced, and concrete was the only structural material used in construction. These ancient structures have been structurally sound for well over a millenium and will be for many years into the future. Ancient engineers designed them such that the concrete only took compressive forces, thus taking advantage of the naturally superior compressive strength of concrete.

As time progressed, engineers found concrete was weak in tension and needed reinforcement to prevent cracking and failure. Adding reinforcement also made the reinforced concrete ductile, reducing the chance of sudden failure. While some plastic and fiber reinforcement has been invented, the vast majority of both new and existing construction is reinforced with ferrous metal, usually low-carbon steel. Furthermore, modern concretes, e.g. portland cement concrete, are designed with water/cement based on workability rather than strength. The increased water content makes modern concrete much more porous and penetrable. As a result, water can move more easily through the cured concrete and will eventually reach the reinforcing steel. In many

older bridges and parking structures, the steel is plain, or unprotected from water ingress. Both factors make the reinforcing steel susceptible to corrosion from water, deicing salts, and other chemicals.

Following decades of neglect, American infrastructure has begun to show its age. Corrosion is now a major problem in RC bridges, docks, parking garages, and other RC structures. Knowing the extent of corrosion is extremely important because it allows engineers to determine the remaining service life of the structure. However, evaluation of facilities in service is difficult and often causes disruptions to traffic patterns, especially in urban areas. Additionally, most of the test methods in use require damaging part or all of the specimen. This is undesirable as it further weakens the structure. In recent years, non-destructive test (NDT) methods have been established for testing the amount of corrosion. One of these is the half-cell potential method (HCP).

The HCP method uses a high impedance voltmeter and a reference electrode to create a current in individual rebars. To create circuit, voltmeter must be connected to one end of the bar and the probe. The probe is then positioned atop the concrete where the measurement is desired. The voltmeter then calculates the drop in voltage that occurs when current travels through the circuit. The potential is then read from the voltmeter; more negative readings indicate a higher probability of corrosion.

Although several NDT techniques can be used, the most widely accepted is the American Standard for Testing and Materials (ASTM) specification C876 "Standard Test Method for Corrosion Potentials of Uncoated Reinforcing Steel in Concrete." ASTM C876 is based on the use of a copper/copper sulfate reference electrode although provisions are made for using a saturated calomel or a silver/silver chloride electrode. The type of electrode does not matter; the only difference between them is the potential

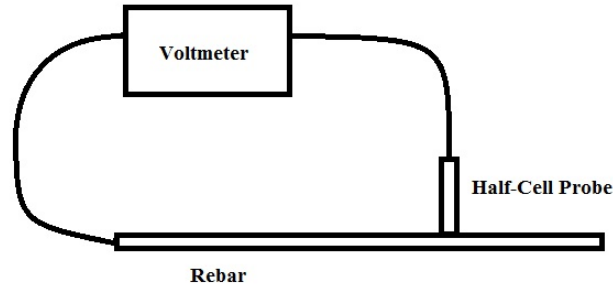


Figure 1.1: Schematic of HCP Test Method

values for different levels of corrosion. Figure 1.1 shows a schematic of the test method. ASTM C876 divides the potentials into three distinct categories. Based on a copper/copper sulfate electrode, values greater than  $-200$  mV indicate the steel has a 10 percent chance of being corroded. Values less than  $-350$  mV indicate a 90 percent possibility of corrosion. Values between  $-200$  and  $-350$  mV indicate the possibility of corrosion is unknown.

Various test apparatuses can be used during the HCP test. Some examples are a single bar embedded in a cylinder [3,23], or multiple bars in beams [17] or slabs [4]. In all cases, accelerated corrosion tests were used to speed the corrosion process. Many experiments included a corrosion inducing current was run through the bars to accelerate corrosion. Chlorides were also mixed into the concrete in some tests. In this thesis, a slightly altered version of the Modified Southern Exposure Test [4] was used with no added chlorides and no corrosion current.

## 1.1 Research Objective

The objective of this thesis is to model the HCP from four RC slabs and to calculate the current density in the bars at the time the measurements were taken. The half-cell potential method is commonly used to estimate the amount of corrosion in reinforcing steel, however there is currently no method to predict future potential values. The importance of cover thickness will also be proved. Furthermore, the current induced when voltage is applied to the reinforcing steel, it increases in density as it travels along the bar if the bar is actively corroding. Thus, the current density can be an indicator of the corrosion state. It is another objective to relate these values to the HCP and use them to predict the state of corrosion at various points along the individual bars.

## 1.2 Thesis Approach

Experimental data sets are collected on four reinforced concrete slabs with rebars all in the same direction; the bars do not overlap and are not electrically connected. The test setup is similar to the Modified Southern Exposure Test. All slabs have the same concrete mix and were cast at the same time. Slabs 1 and 2 have bars in the longitudinal direction, while Slabs 3 and 4 have transverse bars. The only other variable is the thickness of the concrete cover. HCP measurements were taken weekly with a silver/silver chloride reference electrode in accordance with ASTM C876-09.

Analysis is carried out using standard plotting techniques and curve-fitting by regression analysis. Contour plots were created each week to monitor the process. Analysis was done using both the minimum points and average values on each slab. Figure 1.2 shows the layout of the bars in each slab and the overall slab dimensions

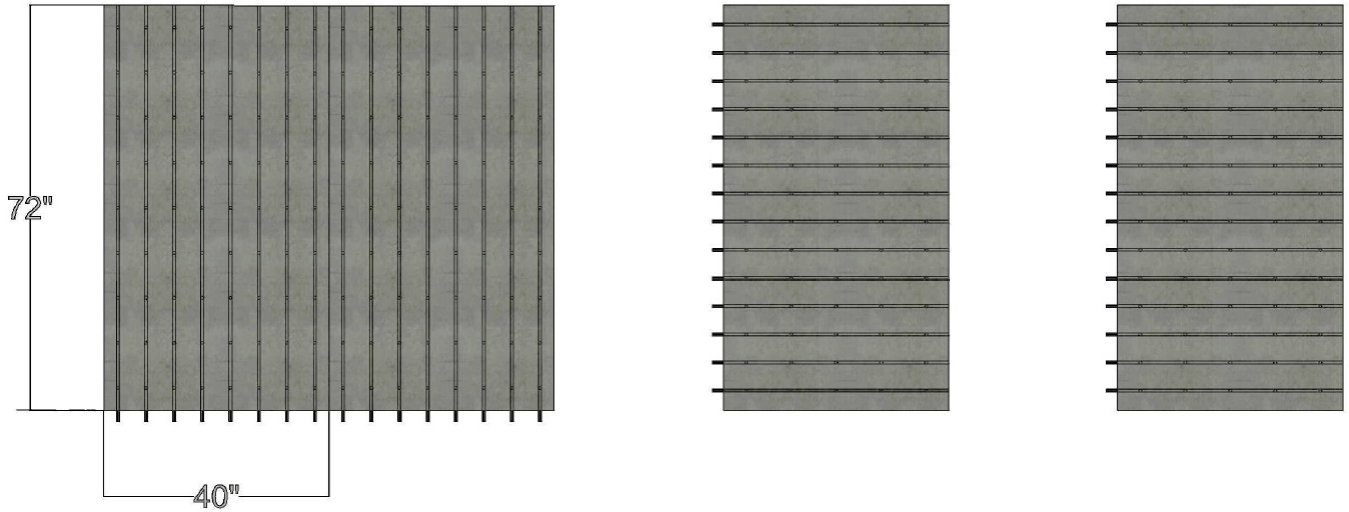


Figure 1.2: Layout of Steel Reinforcement

### 1.3 Organization of the Thesis

**Chapter 2** reviews current knowledge and analysis and findings.

**Chapter 3** discusses the experimental method and testing equipment used.

**Chapter 4** details the experimental findings and further discusses the analysis methods.

**Chapter 5** briefly presents the research conclusions and possible future research work.

# Chapter 2

## Literature Review

Researchers use two approaches to create an accelerated corrosion test (ACT) and monitor the results. The first approach is to create an artificial environment. There are several methods to do this. One involves dissolving salt into the mixing water in varying concentrations. The goal is to make contact between the chlorides and the rebars so corrosion can begin immediately. Another is to pond or soak the specimens in a saline solution until corrosion begins. In this case, chlorides are transported to the rebars with the water as it penetrates the concrete cover. These types of tests usually have elevated, regulated temperature and humidity levels. Corrosion monitoring of half-cell potentials is best done using this method.

The second approach is to induce a corrosion current in the bars. This works by breaking down the passive layer of steel on the surface of the bar and then providing electrons to the oxidation-reduction reaction that causes rusting. This approach is sometimes combined with the previous approach to speed the corrosion process further. Using these techniques, the corrosion process can be shortened from years to months or even weeks. This chapter reviews the current literature available to researchers using HCP to monitor corrosion.

## 2.1 Half-Cell Potential

Batis *et al.* (1997) [1] used the half-cell potential to monitor corrosion in samples of low carbon steel. The specimens were cleaned with hydrochloric acid, acetone, and distilled water to remove any debris before the experiment began. Using a saturated calomel electrode, the authors submerged the specimens and electrodes in a corrosive solution for 160 days. Graphite electrodes were used too. They observed the fluctuation of half-cell and inferred this was because of temperature variation built into the experiment. The Tafel method was used to analyze the results. Potentiodynamic polarization graphs show the log of the corrosion current density is related to the E value. The relationship appears to be almost vertical in the E vs log(i) graph, except for a backwards bend at about -600mV.

Cabrera (1997) [2] demonstrated the ability of formulae to relate crack size to the amount of corrosion. Slabs with three rebars were cast to simulate structural members. The slabs were subjected to soaking for 28 days in a 5 percent NaCl solution. Measurements were taken at 1, 16, and 28 days after the specimens were submerged. The slabs also were subjected to an induced corrosion current with a standard calomel electrode to further accelerate the process. Cabrera found that the bars' cover was the most important factor in corrosion and that the two parameters are inversely related. Furthermore, he proved existing models are accurate for the existing relationship between crack width and pattern and the amount of corrosion. However, these formulae depend on the mass loss in the steel and the density of the rust.

Castro *et al.* (1997) [3] found that accelerated tests accurately predict corrosion in actual environments and the correlation between the artificial and natural environments is linear. To conduct their experiment, the authors cast cylindrical specimens

with a 9.5 mm rebar in the middle. Cylinders were cured for 7 days. An activated titanium rod was used to monitor corrosion potential and was calibrated against a saturated calomel electrode. Field specimens were positioned vertically 50 m from the sea whereas the lab specimens were subjected to continuous 5% NaCl spray. Analysis indicated that the corrosion current tapers off to  $10 \mu A/cm^2$  after 24 months of field exposure. This point is independent of chloride content in the concrete. After the rebar reaches an active state, it will corrode regardless of the amount of chlorides in the concrete. Additionally, the corrosion current vs. time curve correlates well by the following equation:

$$\log(I_{corr}) = A + B * \log(t) \quad (2.1)$$

where A and B are constants.

Ohtsu and Yamamoto (1997) [21] concluded the HCP method is reliable for detecting corrosion in concrete if a modified version of the boundary element method (BEM) is applied to the HCP measurements. The modified approach is called the charge simulation method (CSM). The BEM is based on a boundary integral, which has been broken up into a square mesh. The potential and current are then input into each element and all the elements are summed. The CSM, or indirect BEM, uses a virtual boundary to eliminate irrelevant solutions. Care must be taken when applying the CSM to edge bars because it does not account for media besides steel and concrete. Applying CSM to HCP measurements in conjunction with the corrosion criteria in ASTM C876 gives accurate predictions of corrosion in rebar. An accelerated corrosion test with an applied current was run; the slabs were ponded with a 3 percent NaCl solution. The experimental analysis verified the theoretical results.

Darwin *et al.* (2001) [4] compared the Southern Exposure Test and the Modified

Southern Exposure Test methods available to researchers. The Southern Exposure Test consists of a slab with two mats of reinforcing bars; the top mat has two rebars and the bottom has four. The layers are electrically connected using a 10 ohm resistor and are ponded in weekly cycles with a 15 percent NaCl solution for 48 to 96 weeks. The temperature during ponding is set to 72 degrees Fahrenheit and when wet and 100 when dry. Forty-eight weeks approximates 30 to 40 years of corrosion in bridge decks. To evaluate corrosion, they used the half-cell potential method. It is based on a copper/copper sulfate electrode and ASTM C876. It is difficult to relate HCP to corrosion rate because this method cannot differentiate between macro and microcell corrosion. Furthermore, the results should be checked with another test method. Finally, the test results are only good for the environmental and specimen conditions of the test.

Elsener (2001) [7] described the use of half-cell potential for analyzing repairs to concrete bridge decks. All experiments were performed with a copper/copper sulfate electrode in accordance with ASTM C876. His results showed that after the bars were cleaned and new concrete was placed over the bars, the HCP decreased while the concrete was cured; HCP then increased showing the rebars had regained their passive state. Positive shifts of more than 100 mV were recorded indicating that heavily corroded areas had been repaired and the corroded rebars now behaved like new rebars. Elsener also found that the HCP measured on the rebars were typically lower than the values measured on the surface of concrete.

Li (2001) [16] used both full-scale and model RC specimens to test the effects of salt spray on steel reinforcement in a controlled environment. The NaCl content was 3.5 percent to simulate seawater. A copper/copper sulfate electrode was used to measure HCP according to ASTM C876. The HCP readings were reliable because the

conditions were controlled. Crack initiation and corrosion in concrete were related to crack size. The chloride penetration varied greatly with concrete cover depth for cracks smaller than .1 mm. However, specimens with larger cracks had no significant correlation with concrete cover depth.

Pech-Canul and Castro (2002) [23] found that the corrosion potential generally decreases with time but also fluctuates widely. They also found that corrosion current density generally increases with time. To conduct their test, they cast several .5 w/c concrete specimens with a #3 rebar embedded in the center of each one. The ends of the specimens were coated with epoxy and the counter electrode was placed on the perimeter of the specimen. The HCP values were measured against a saturated calomel electrode. Once cured, the specimens were placed 50 m from the shoreline. The test was run for 56 months. Results show that corrosion began after about 6 months and HCP significantly decreased. The specimens passed the 90% corrosion probability after about 23 months. But HCP increased into the uncertain range by month 27 before decreasing and increasing again. Current density generally increased with time.

Gonzales *et al.* (2004) [9] found that the HCP values vary widely based on the moisture content of concrete at the time of drying. The test consisted of two 10 or more year-old cement mortar slabs containing 13.8 mm (about the size of a #3 bar) spaced 9 cm on center. One slab was mixed with 3% added chloride. The slabs were initially wet with damp cloths placed over a small part of the slab for 7 days and a corrosion current was run through the rebars. After 7 days, damp cloths were placed entirely over both slabs for the remaining 21 days of the test. All measurements were made with reference to a saturated calomel electrode. HCP values remained fairly steady at about 300 mV for the first 7 days of the test, then dropped rapidly

thereafter. The HCP continued dropping until the end of the test. They found that the moisture content affects the HCP readings regardless of the chloride content (because the increased moisture decreased resistance). The HCP differences observed were several hundred millivolts. They also recommended that ASTM C876 needs to be revised based on their findings. They also suggested the use of another parameter, such as current density should be considered to verify HCP readings.

Leelalerkiet *et al.* (2004) [15] proposed a method to test the validity of half-cell potential as a measure of corrosion in concrete. In the tests, small concrete specimens were cast with six rebars according to ASTM C876, the standard for measuring half-cell potential. They used a silver/silver chloride electrode and corrected the HCP measurements to copper/copper sulfate values. They terminated the experiment when all HCP measurements were below -350 mV, after a period of 63 days. The ponding cycle lasted for 1 week; specimens were placed in both fresh water and saline solution with a 3 percent NaCl content. Upon visually inspecting the specimens, they found that the HCP was not a good indicator of corrosion because the rebars were far less corroded than predicted. Thus, the inverse boundary element method was needed to modify the HCP measurements to accurately predict the corrosion of embedded rebars.

Li and Melchers (Sept.-Oct. 2005) [17] made 30 reinforced concrete cantilevers using different mix proportions and tested the cantilevers for the effects of corrosion under service loads. To simulate a marine environment, a sprayer was used to spray the cantilevers according to ASTM C876. The cantilevers were evaluated by destructive testing at the end of the experiment. A statistical analysis revealed that the rebar diameter did not make a significant difference in factored load resistance once corrosion started. In conclusion, they found that marine environments affect

structures' servicability before significantly affecting structural strength.

Hussain and Ishida (Unpublished Manuscript, 2006) created a finite element analysis (FEA) to simulate mass transport of chlorides in concrete. They found that in the presence of chlorides, the passive  $Fe_3O_4$  coating on the steel breaks down and active corrosion begins. Their test used chlorides dissolved into the mixing water with varying concentrations of 0 to 10 percent by mass of binder. They found that the two most influential factors in both corrosion rate and HCP were i) the chloride concentration and ii) the experiment temperature.

Poupard et al. (2006) [24] exposed a prestressed concrete beam to saltwater spray to study the effect of saltwater spray on reinforced concrete. The beam was placed such that the tension side was on the top and the service loads did not put the top in compression. Using HCP measurements, they found corrosion was most likely in the tension zone. Upon destructive testing, the hypothesis was proven correct. Hairline cracks in the concrete because of prestress caused the large amount of corrosion. The HCP corrected using the RILEM recommendations yielded very accurate correlation between the HCP and the actual corrosion. The anode had more corrosion than the cathode. Chloride concentration was found using phenolphthalein and titration of chlorides recovered from the phenolphthalein solution.

Maruya *et al.* (June 2007) [19] calculated the HCP by modeling the mass transport of chlorides and oxygen through concrete. The experiment consisted of concrete slabs exposed to salt spray from the ocean for about four years. From their calculations, they observed that HCP decreases after the initiation of corrosion, but increases and stabilizes after the concrete cracks. HCP were different at various points along the rebars due to the chloride and oxide concentrations. It was also discovered that corrosion at one point will cause HCP fluctuations along the rebar. Furthermore, the

current density was calculated using the following formula:

$$I_i = \frac{1}{B\Delta L_i} \sum_{j=1}^n \frac{\delta E_{i,j} B \Delta L_j}{w \delta L_{i,j}} \quad (2.2)$$

in which  $I_i$  is the current density at one point on the bar,  $B$  is the width of the bar,  $E$  is the potential difference,  $L$  is the length of the element, and  $w$  is the specific resistivity of concrete. In this thesis,  $w$  is taken to be 31.5  $\Omega$ in.

Yuan *et al.* (2007) [31] compared the galvanostatic method and an artificial environment to see the methods' effects on the corrosion of reinforcing steel and the mechanical properties of RC beams after corrosion. They subjected the beams to a three-point bending test after corrosion. A 5 percent NaCl solution was used in the artificial environment. Two normal rebars were used as anodes and a stainless steel bar was used as the cathode. The artificial environment produced more natural results, but the corrosion process took longer. For corrosion-induced cracks of 0.02 inches or less, the beams failed in flexure, like the non-corroded beam. However, a beam with a 0.032 inch crack suffered a brittle failure. Furthermore, the artificial environment produces corrosion patterns more consistent with those found in existing structures.

Muralidharan *et al.* (2008) [20] used an embedded  $MnO_2$  sensor to monitor HCP. The measurements used a saturated calomel electrode. All the HCPs were very high, about positive 200 mV. However, the results were reasonable when converted to copper/copper sulfate values. Experimental results showed a passive HCP was -312 mV for a cube with no chlorides in the mix. Active HCP was about -532 mV for a three percent chloride content. The test specimens were exposed to natural conditions for about 1 year. Further tests showed that corrosion current was between  $2.27 \times 10^{-5}$  and  $3.27 \times 10^{-5} A/cm^2$  based on chloride content.

Yuzer *et al.* (2008) [32] derived a formula to predict the time required to see

cracking on the surface of concrete as a function of i) the silica fume and chloride concentrations and ii) the loss in rebar diameter. The results were taken from an accelerated corrosion test using concrete cylinders with one 10 mm rebar embedded in them. Different chloride concentrations were dissolved into the mixing water. Different concentrations of silica fume were added to concrete. A steady current was applied to the rebars for 7 days and the change in current density was monitored. Formulae were derived using a regression analysis based on the total current delivered to the rebar over the 7 days (the area under the current density vs, time curve). Corrosion was assumed to be uniform over the entire surface area of the rebar. The final equation was:

$$t = L * \frac{[1211.608 + 16.803 * [SF] + 4.580 * [Cl^-]]}{1806 * 10^{-004}([Cl^-] - [SF])} \quad (2.3)$$

where  $L$  is the critical rebar diameter loss,  $[Cl^-]$  is the chloride concentration, and  $[SF]$  is the silica fume concentration.

Gulikers (2009) [10] applied a statistical approach to find the likelihood of corrosion from HCP measurements. Using a copper/copper sulfate electrode and a parking garage, he prewetted the concrete to ensure good conductivity. After applying a regression analysis to the data, a best fit line was obtained. He found that the cumulative frequency distribution was less pronounced than a simple frequency distribution for predicting corrosion. He also noted that a large amount of data is required for an accurate analysis.

Reou and Ann (2009) [26] compared the galvanic current and the HCP techniques for measuring corrosion of embedded rebars. The experiment was designed using a single bar within cast concrete specimens. Specimens were cast with 0, 0.5, 1, 2, and 3% NaCl concentrations by mass of cement. After a full 28 day cure, the specimens were subjected to weekly ponding cycles for 15 weeks. HCP measurements were taken

with a standard calomel electrode every week for 15 weeks. The corrosion rate was calculated as follows:

$$I_{corr} = \frac{B}{R_p} \quad (2.4)$$

$B$  represents the corrosion potential and  $R_p$  is the polarization resistance. They found that the chloride content of the concrete had no effect on the HCP. They also found that spikes in the galvanic current indicate the onset of corrosion.

Otieno *et al.* (Sept.-Oct. 2010) [22] tested the resistivity of concrete, HCP, and linear polarization resistance for their correlation to corrosion in concrete. Using a silver/silver chloride electrode, HCP measurements were performed for 32 weeks on cracked and uncracked beams using a 5 percent NaCl solution. Concrete cover for all rebars was 1.6". The cracked specimens showed corrosion almost immediately because water flowed into the crack. ASTM C876 was followed when conducting the experiment. A moving average was used to evaluate the HCP data. In the end, concrete corrosion rates were linked reliably to corrosion rates. However the authors cautioned against using lab data to represent field conditions. Furthermore, they recommended using more than one method to ensure correct results.

Guzman *et al.* (2011) [11] developed a finite element method (FEM) to simulate the cracking of concrete due to chloride penetration in concrete slabs. Penetration is based on Fick's Second Law using an average diffusion coefficient for concrete simulated as a heterogeneous materials. A highly porous area was placed around the rebar and this was allowed to fill with rust before stress and strain were induced in the concrete. Section loss of the rebar was considered. Using a previous accelerated corrosion test to test their code, they found the FEM accurately modeled the crack pattern around the rebar. The pattern was as follows: at first, the cracks are small and appear around the entire rebar. Then, some of the cracks lengthen until they

become significantly longer than others. Finally, the longest cracks appear on the surface of the slab.

Hussain (2011) [12] ran an experiment to find the corrosion potential of ponded concrete specimens with varying cover over one year. Keeping the rebar size (0.52" diameter) and temperature constant (20 centigrade), concrete covers were set to 1.575 and 2.755 inches. A copper/copper sulfate reference electrode was used to take readings in accordance with ASTM C876-91. HCP readings only changed gradually throughout the ponding cycle. Furthermore, he found that the rebars with less cover show sharp increases in HCP at the start of the wetting cycle. Afterwards, the HCP values still increase but at a much slower rate. He infers that this is because of the relatively short time it takes for the chloride solution to reach the rebars.

Pradham and Bhattacharjee (2011) [25] conducted a test relating the amount of chlorides in concrete to the HCP and the corrosion current. Their experiment consisted of slabs with varying w/c ratios and steel types. Chloride was added to the concrete mix. Using a saturated calomel electrode, they took measurements according to ASTM C876 and modeled the corrosion rate using linear polarization resistance measurement. They found that as the chloride content was increased, the HCP dropped in all specimens. When the experiment was finished, all slabs made with ordinary portland cement (OPC) and w/c = 0.5 were actively corroding. Thus, HCP was found to be a good indicator of corrosion. Furthermore, they found that there was no correlation between chloride content and corrosion current. Thus, whether chlorides were in the mix or penetrated into the concrete makes a difference during corrosion.

Duffo *et al.* (2012) [5] performed a non-accelerated corrosion test on reinforcing steel embedded in 2" of concrete. Using HCP based on a copper/copper sulfate

reference electrode, they found that there is no significant change in HCP after 1,600 days. They noted that the corrosion potential remains nearly constant, around -200 mV, but there is a slight uptick in HCP as time goes on. Measurements were taken according to ASTM C876. Additionally, corrosion current density was calculated according to the  $R_p$  (see equation 2.4) values. When compared to HCP, the corrosion current seemed to be constant while HCP increases throughout the experiment. A possible reason is that corrosion was not accelerated. Therefore, results occur much slower than in a Modified Southern Corrosion Test.

LNCE (2012) [14] found an inverse relationship between the concrete resistivity and the corrosion rate. They also reported that both the degree of saturation and concrete cover influence the corrosion potential. Also, the HCP can not be directly related to the corrosion rate, but Faraday's Law should be used. Based on the RILEM recommendation, corrosion rates for different current densities are estimated as:  $>0.39$  A/sq. in. indicates high corrosion,  $<0.039$  A/sq. in. indicates negligible corrosion, and between 0.039 and 0.39 A/sq. in. indicates low or moderate corrosion.

## 2.2 Current Density

Kranc and Sagues (2001) [13] developed a FEM for the analysis of corrosion in mats of rebars. The model was based on the anodic and cathodic reactions between molecular oxygen, water, and the iron in the steel rebars. The model was applied to rebars in both the horizontal and vertical directions and accounted for the connection between layers of rebars. Rebars were modeled with nodes placed at the center of the rebars. All potentials for the model were based on the saturated calomel electrode. Additionally, corrosion potential values were taken as positive throughout the paper. They ran tests to prove the accuracy of the model. From the test results, contour

maps were drawn on the reinforcing mat to provide a picture of the state of corrosion of the bars.

Zhang *et al.* (2001) [33] derived a method to evaluate the corrosion of embedded rebar using the complex resistivity and impedance. The resistivity was based on the geometry of the specimen. As the current travels through the rebar, there is less resistance. Once the current enters the concrete, resistance is comparatively high. The impedance calculation was based on the critical frequency. This frequency is the same for a specimen regardless of rebar cover. The model predictions were verified with experimental results. Specimens were cast and placed in a calcium hydroxide solution before HCP measurements were taken. The experimental results agreed with the theoretical model.

Trejo and Pillai (2003) [29] developed a new test to accelerate the corrosion of steel embedded in cement mortar. The ultimate objective was to determine the service life of concrete structures. Cement mortar specimens were cast and cured before being exposed to chlorides. An electric current was run through the rebars with voltages from 5 to 40 volts. However, only the specimens subjected to 20 or 40 volts were useful in further testing. After completion of the test (4-5 weeks), the specimens were broken and the paste bonded to the rebar was subjected to a pH test to determine its chloride content.

Trejo and Palli (Feb. 2004) [30] used an accelerated chloride threshold test to find the chloride concentration needed on the steel surface to initiate corrosion. Micro-composite, SS304, and SS316LN steels were tested and compared to the ASTM A615 and A706 steels. Because the corrosion-resisting steels were alloyed with other metals like chromium and nickel, they needed a much higher chloride concentration to initiate corrosion. Chloride thresholds are given below in lb/cu.yd. of chlorides. These

results are at the 95 percent confidence level: A706 - .3, A615 - .9, Microcomposite - 7.7, SS304 - 8.5, SS316LN - 18.1

Topcu *et al.* (2009) [28] created an artificial neural network (ANN) that can model data from an accelerated corrosion test. An ANN is basically a computer algorithm that functions much like a human brain in that it can learn and think. To conduct the test, they used 150 x 300 mm cylinders with a 14 mm rebar embedded in the cylinders. The cylinders were cured for 28 to 180 days to investigate the effect of curing time on the corrosion current. The cylinders were subjected to a corrosion current in a bath containing 4% NaCl. Increased cure time leads to a decrease in corrosion current required to corrode the rebars. In the end, the ANN accurately fit the data to a linear curve.

Sandowski (2010) [27] created a new NDT method to find the corrosion rate in concrete without removing the cover from the rebars while the member is in service. This new NDT method used a short circuit to find the resistance of the rebar and concrete and used the corrosion current density to determine the corrosion rate. To test his method, three RC slabs were cast with a single rebar embedded in the slabs and exposed to the atmosphere on each end. The concrete covers for the rebars were 10, 20 and 30 mm. The slabs were then subjected to an accelerated corrosion test. In the test, both DC and AC testing methods were used simultaneously. The test showed that if the induced DC is about equal to the AC of the bar, then the bar is actively corroding. However, if the DC is close to the AC of the concrete, then the rebar is still passive.

Lu *et al.* (2011) [18] derived a theoretical equation for the cracking of concrete due to the increase in rust volume developed around the reinforcing steel. They included several factors previous researchers ignored such as the volume of the cracks and the

mechanical properties of several types of rust. Like many others, Their formula was based on the mass loss of the steel rebar after subjecting the rebar to an accelerated corrosion test. They used the molecular weight of various corrosion products to calculate the rust volume generated when the crack occurs. These volumes are then correlated to the amount of steel in the concrete and the mechanical properties of the steel. They also concluded that an increase in rebar diameter reduces time to cracking because it reduces concrete cover.

Doung *et al.* (2013) [6] found the HCP and the corrosion current density may not be accurate for detecting corrosion. Their experiment involved casting rectangular concrete prisms containing rebars and water flowing over the specimens in a wet/dry cycle. HCP measurements were taken every 30 days according to ASTM C876. The concrete cover for the corroding rebar was 10 mm. HCP was measured using a copper/copper sulfate electrode and current density was measured by a 100  $\Omega$  resistor and a voltmeter. After 480 days, none of the specimens had an HCP below -350 mV. Furthermore, the corrosion current indicated that there was no corrosion. However, when the specimens were visually inspected all the rebars were severely corroded. They questioned the validity of the results.

## 2.3 Summary

Although some researchers found that HCP is not always reliable, many more researchers found that HCP and current density can accurately describe are good indicators of the level of corrosion in concrete. The two most common test methods are i) ponding/mixing chlorides into the concrete and ii) using an induced corrosion current. In this chapter, previous work was reviewed and classified based on the type of test.

# Chapter 3

## Experimental Method

In this chapter, the experiment and the methods used to gather data are described. In this accelerated corrosion test, no electric current was applied to the bars to further accelerate corrosion. The level of corrosion was monitored using a half-cell potential sensor. The test equipment was an Elcometer (TM) 331 Model H.

### 3.1 Half-Cell Potential Voltmeter

The voltmeter consists of a battery, a probe, and several clips. The battery pack has an illuminated display and takes readings in millivolts. Several options are available to modify the data based on external conditions such as rain, however none of these options were used in this experiment because the test was run in a controlled environment. The battery is rechargeable and the system comes with a cable for recharging the battery. The battery usually lasts six weeks before a recharge is needed. On the front of the unit are two docks for the probe and the alligator clip to connect to the rebar. The housing is made from a plastic that is not affected by the presence of corrosive materials and is held together with stainless steel screws.



Figure 3.1: Half-Cell Sensor

The two 5.5' cables that come with the system link the voltmeter to the rebar and the probe. Both contain stainless steel contacts that insert into the voltmeter. The black wire then connects to the probe with another stainless steel contact. The red wire features an alligator clip that connects to the wires protruding from the rebar. Both are covered in a plastic insulation to prevent corrosion from the environment.

Either a copper/copper sulfate or a silver/silver chloride probe comes with the system. In this test, a silver/silver chloride probe was used. The probe resembles a wand and connects to the voltmeter via the aforementioned wire with a stainless steel contact. A rubber cap is placed on the end of the probe to protect it from the environment when the probe is not in use. The cap is removed while taking measurements. Both ends of the probe are rounded and sufficient contact must be made between the base of the probe and the concrete surface. To get an accurate measurement, the probe must be placed vertically and come in full contact with the concrete surface.

Some sources of error when using the system are:

- 1) **Bad connection to rebar**
- 2) **Bad connection to voltmeter**
- 3) **Probe not vertical**

## **3.2 The Slabs**

Four slabs measuring 40 x 72 x 7 inches were cast using commonly found mix materials. Ordinary Type I Portland Cement was used as a binder. The water content was 325 lb/yd<sup>3</sup> making the water/cement ratio .51. Coarse aggregate consisted of pea-stone with a maximum size of .5"; the unit weight was 1727 lb/yd<sup>3</sup>. Fine aggregate consisted of fine sand with a unit weight of 1105 lb/yd<sup>3</sup>. Final mix proportions are 564 lb/yd<sup>3</sup> cement, 1600 lb/yd<sup>3</sup> of both gravel and sand, 35 gal/yd<sup>3</sup> water, and 16.9 oz/yd<sup>3</sup> water reducer. The final slump was 1". All slabs were made from the same mix.

Reinforcement consists of #4 uncoated rebars in two layers. The bottom layer is located one inch from the bottom of the slab. The top layer varies in depth from 1.5 to 2.5". Slab One has eight longitudinal rebars placed 5" on-center; all bars have 1.5" cover. Slab Two also has eight longitudinal bars, but has 2.5" cover for all bars. Slab Three has fourteen transverse bars spaced five inches on-center. The cover varies among three sets of bars. The first set has four bars and a cover of 2.5"; Set Two has five bars at 2" cover; and Set Three has five bars at 1.5" cover. Slab Four has the same dimensions and configuration as Slab Three. All bars extend beyond the concrete, but the ends are epoxy coated to prevent corrosion. Stripped wires are welded to the bars so a connection to the half-cell system can be made. All slabs were allowed to cure for 28 days before testing began.

Slabs 1-3 have dams made from acrylic sheet to keep the pond water on them

during the ponding cycle. Slabs One and Two are adjacent to each other so the dam is serves both slabs. A buffer os silicone prevents chloride migration between the slabs. Slab Four has no dam because it is not ponded. The acryillic sheets are held together with silicone and are attached to the slabs with the same material. Slabs Three and Four are standalone and do not have any contact with the others.

### **3.3 Test Procedure**

The test procedure Follows a modified version of the Modified Southern Exposure Test. Testing began on Fridays when the slabs were ponded using a 15% NaCl solutuion. The solution was placed on Slabs 1-3 and left inplace for four days. On Tuesday, the solution was removed from the slabs and they were allowed to dry for three more days. slabs were prewetted several hours before taking measurements. On Friday, the measurements were taken according to ASTM C 876-09 "Standard Test Method for Corrosion Potentials of Uncoated Reinforcing Steel in Concrete."

To take measurements, the HCP device was set up according to the manufacturer's instructions. After the slabs had been sufficiently prewetted, the alligator clip was fastened to the stripped wire. A damp cloth was placed under the probe while measurements were being taken to ensure good conductivity between the probe and the slab. The probe was laced over the bars and HCP values were recorded on specially made data sheets. measurements were taken every eight inches alont the bar and were always directly over the bar. Slabs One and Two had 9 measurements per bar for a total of 72 measurements per slab. Slabs Three and Four had five measurements per bar for a total of 70 measurements per slab. Testing continued for 52 weeks.

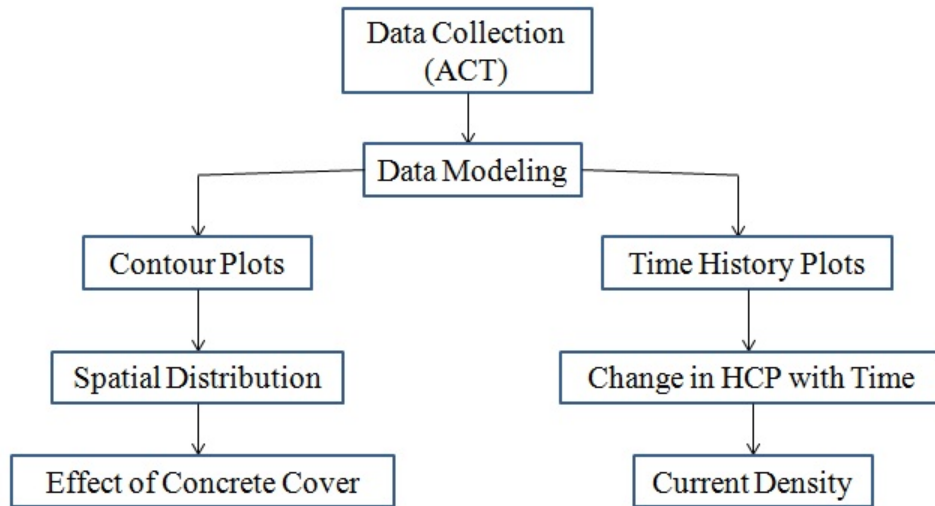


Figure 3.2: Methodology of the Thesis

### 3.4 Summary

This section describes the half-cell measurement system, the slabs, and the experimental method. The mix proportions of the concrete are also detailed. Moreover, the reinforcement scheme and relative positions of the slabs are described. Finally, the ponding cycle and method and details of gathering data are discussed.

# Chapter 4

## Experimental Results

Results from the accelerated artificial corrosion test are divided into two parts. First, the actual HCP measurements yield the development of corrosion on each slab both spatially and temporally. Additionally, the HCP results allow us to plot the time history of the current density on each bar for every slab. During the ponding cycle the temperature was set to 100°F when the RC slabs were ponded and was reduced to 72°F during the drying cycle. The results were analyzed for consistency in the data to predict the future values of the parameters studied. In this experiment humidity, saline content, duration of the ponding cycle, size and type of rebar, and concrete mix proportions were held constant. The only variables were the concrete cover and the temperature (variations were required in the test specification, but are not considered in the analysis). The results clearly show the relationships between HCP, time, and current density. From these relationships, characteristic equations were derived to accurately describe the relationships. All these equations have reasonable correlations with the experimental data and were obtained within the 95% confidence interval.

## 4.1 Time-Dependent Half-Cell Potentials

When reinforcing steel is first placed in concrete, there is no corrosion and the steel is protected by both the concrete cover and a passive layer on the steel itself. However, as time progresses water and chlorides penetrate into the concrete and cause the passive layer to break down through a series of chemical reactions. The breakdown in the passive layer is permanent and can not be reversed except by removing the concrete cover and cleaning the steel. The bars were not cleaned at any point during the test. Curve-fitting analysis was performed using a cubic polynomial following the equation:

$$HCP(t) = P_1t^3 + P_2t^2 + P_3t + P_4 \quad (4.1)$$

The following sections discuss and give parameters for each slab individually.

### 4.1.1 Slab 1

From the HCP measurements, Slab 1 behaved largely as expected throughout the test, although the half-cell potential values increased slightly in the first few weeks. This may be due to remaining curing water on the surface of the concrete at the time the measurements were taken; even small amounts of water are known to have an effect on HCP values. Analysis was done using both the minimum and the average HCP values recorded each week. The minimum HCP was selected because it indicates the most corroded location on the slab. The average HCP was chosen to describe the slab's overall behavior. The half-cell potentials steadily decreased with time as indicated by the contour maps in Figures 4.1-4. Measurements are in millivolts.

Additional HCP analysis gave more concrete results about the location where corrosion began. Figure 4.5 shows the min, average, and maximum HCP values with time. The decreasing trend began at about week 18 for the minimum HCP value.

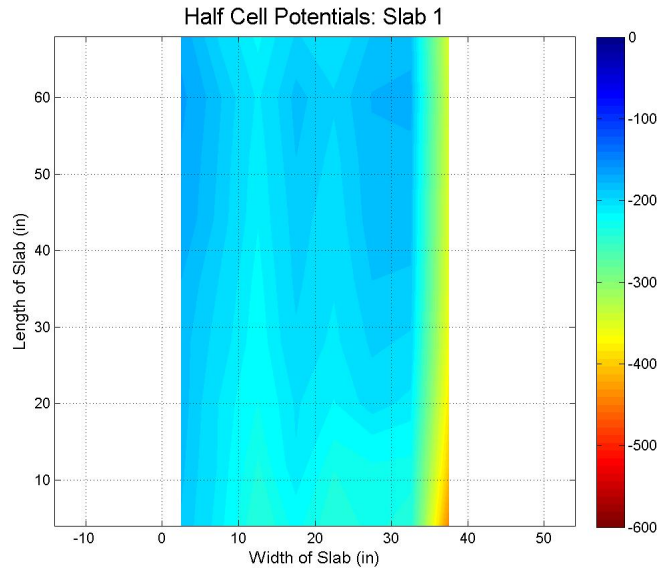


Figure 4.1: Contour Map of Slab 1 on 23 March 2012, Week 11

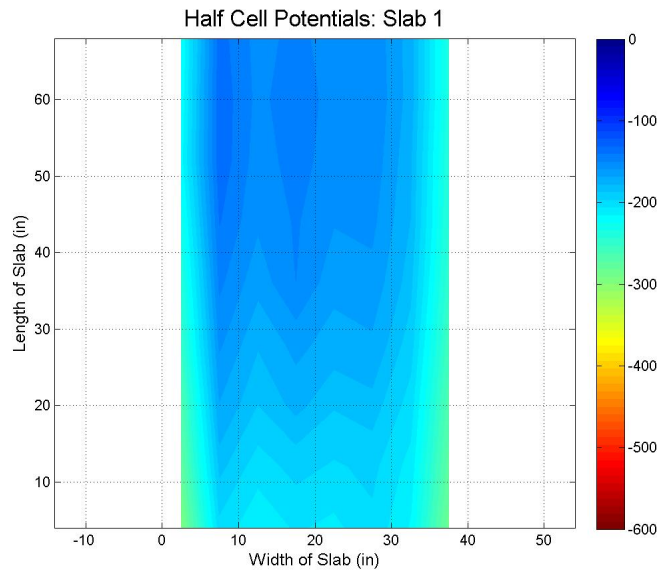


Figure 4.2: Contour Map of Slab 1 on 25 May 2012, Week 20

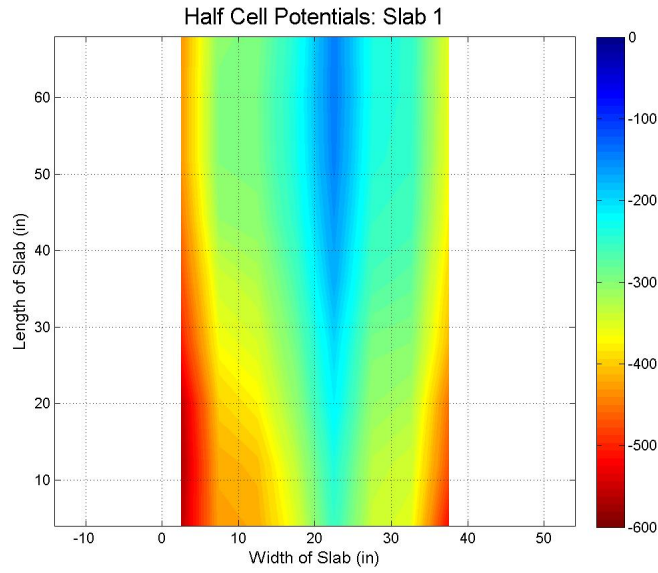


Figure 4.3: Contour Map of Slab 1 on 10 October 2012, Week 40

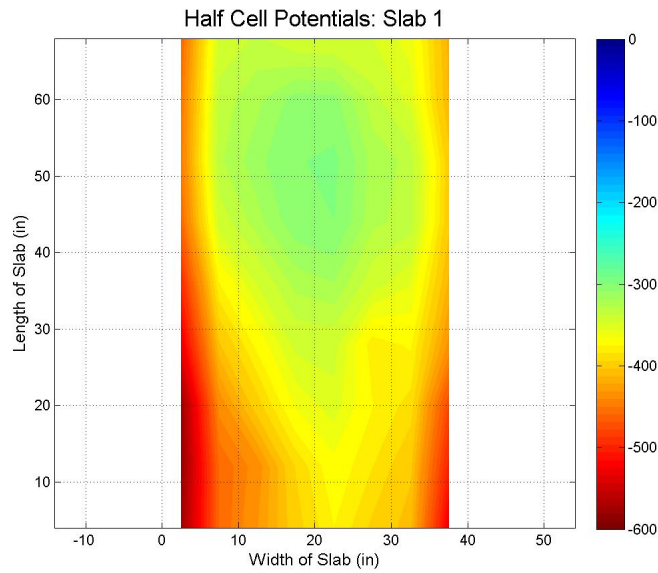


Figure 4.4: Contour Map of Slab 1 on 4 January 2013, Week 52

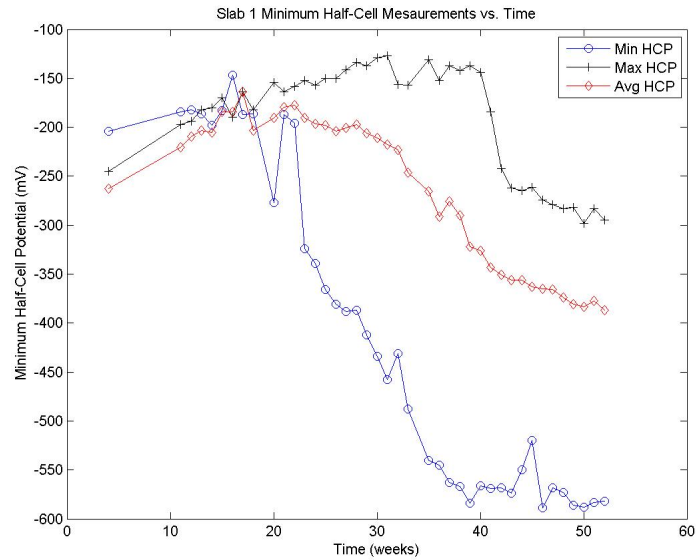


Figure 4.5: Minimum, Average, and Maximum HCP as of Week 52

The minimum began to settle out at week 39 because the surface area of the rebar was so reduced, there was less contact with the chlorides. Thus, the decrease in HCP slowed. The lowest HCP value recorded in week 52 was about -580 mV. The average values followed a similar trend, except the slope of the line is reduced. Average HCPs also began to decrease about week 18 and saw a reduced slope beginning at week 43. The average HCP finally reached a value of about -300 mV after 52 weeks. The maximum HCP was plotted for comparison purposes only and was not considered in the analysis.

Figure 4.6 shows the results of curve fitting for the minimum HCP fit by a cubic polynomial. A series of "x" represents the data points and the dashed lines represent the 95% confidence intervals. Figure 4.7 shows the average data. The parameters for these equations are given in Table 4.1.

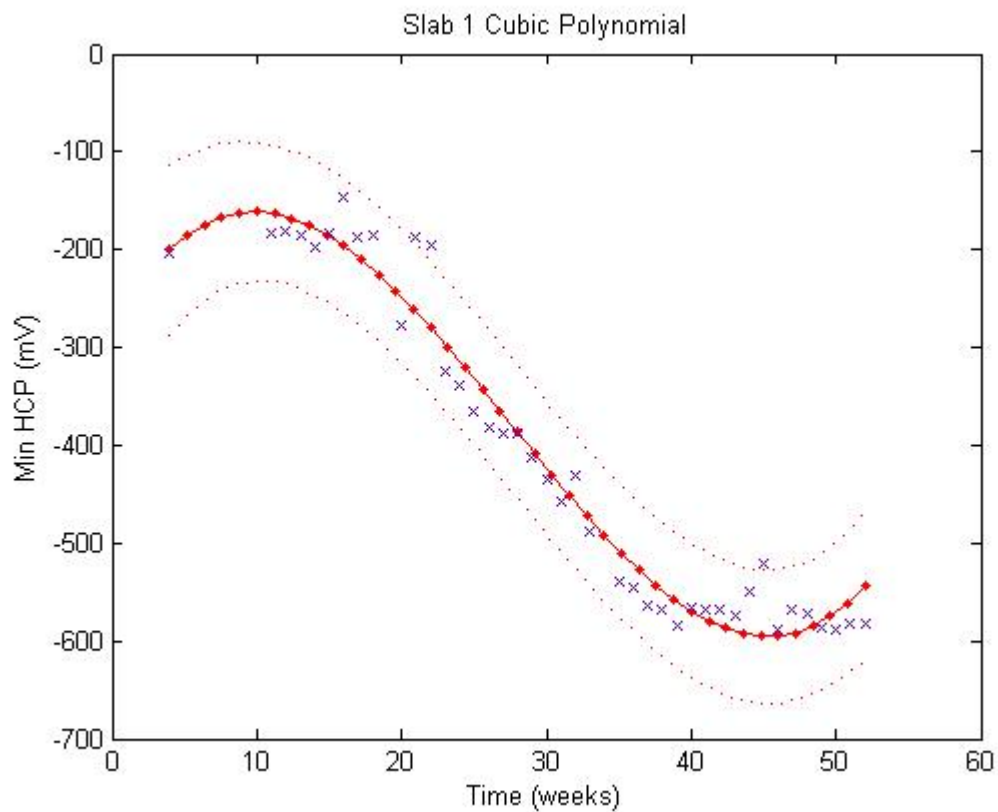


Figure 4.6: Minimum HCP Data and Cubic Polynomial as of Week 52

Table 4.1: Parameters for Slab 1

Measure	P1	P2	P3	P4	R Square
Minimum	.01942	-1.606	25.91	-279.2	.9627
Average	.007496	-.8519	23.51	-370.2	.9697

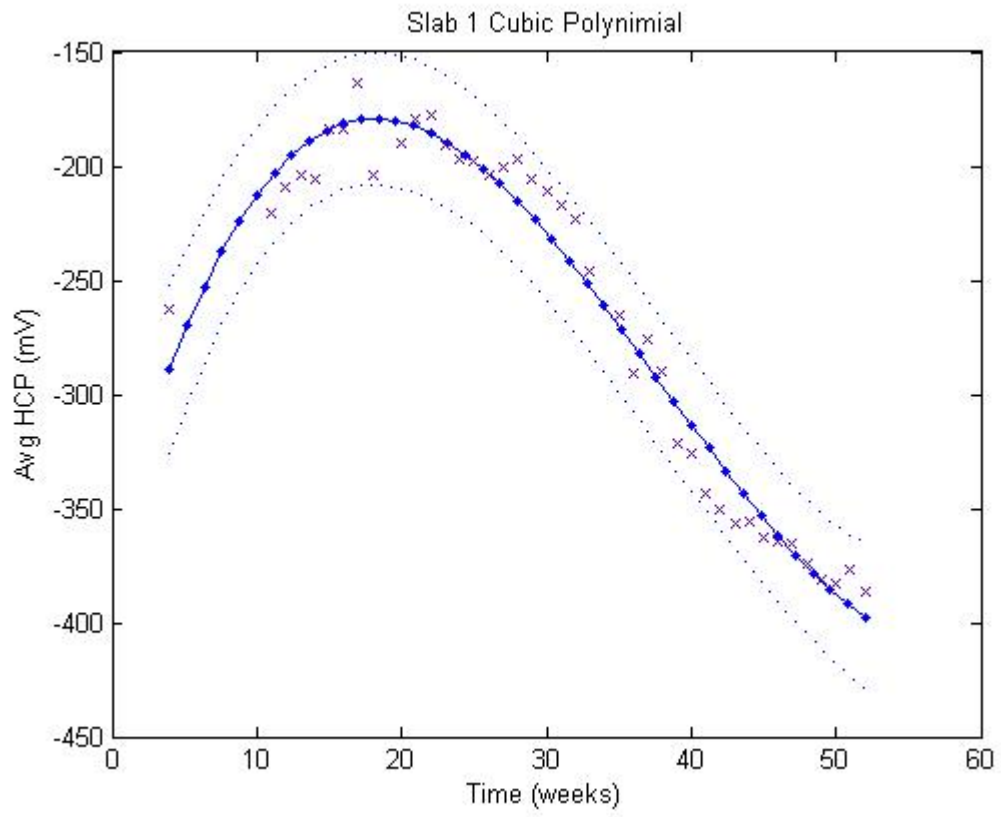


Figure 4.7: Average HCP Data and Cubic Polynomial as of Week 52

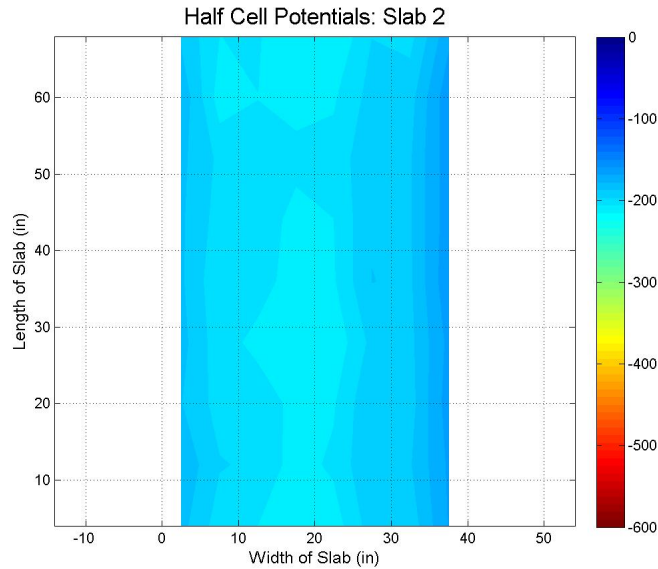


Figure 4.8: Contour Map of Slab 2 on 23 March 2012, Week 11

#### 4.1.2 Slab 2

Slab 2 did not experience any major increase or decrease in its HCP measurements during the experiment. The overall HCP trend was steady while slightly increasing with time. At the start of the test, the HCP was about - 210 mV; this rose about -180 mV by week 52. The most likely cause for the overall HCP trend is the depth of the rebars. 2.5 inches of concrete cover was placed on the rebars; since no rust was observed on the surface of the slab, it is believed that the concrete cover was not fully penetrated during the ponding cycle. The slight increase in HCP may be a result of noise unintentionally included while taking HCP measurements. More on this will be discussed in the subsection about Slab 4. Overall, Slab 2 was the most consistent of the four RC slabs and can be used as a benchmark for the other slabs in the experiment. Figures 4.8 through 4.11 show contour maps from the same weeks as those in the previous section. Measurements are in millivolts.

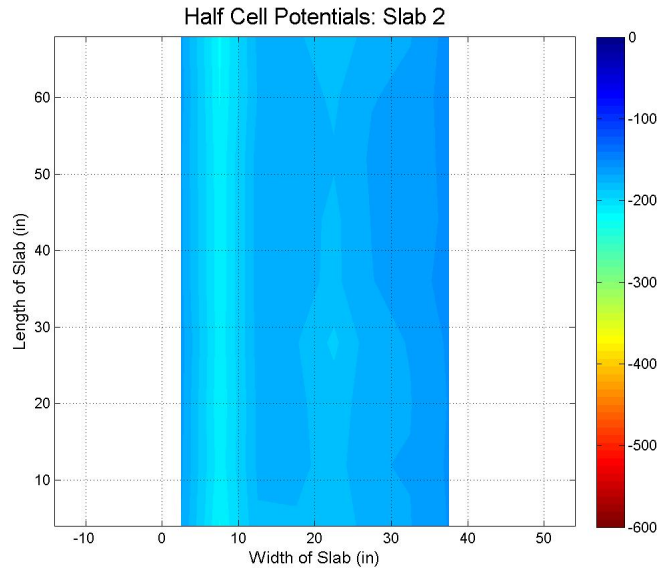


Figure 4.9: Contour Map of Slab 2 on 25 May 2012, Week 20

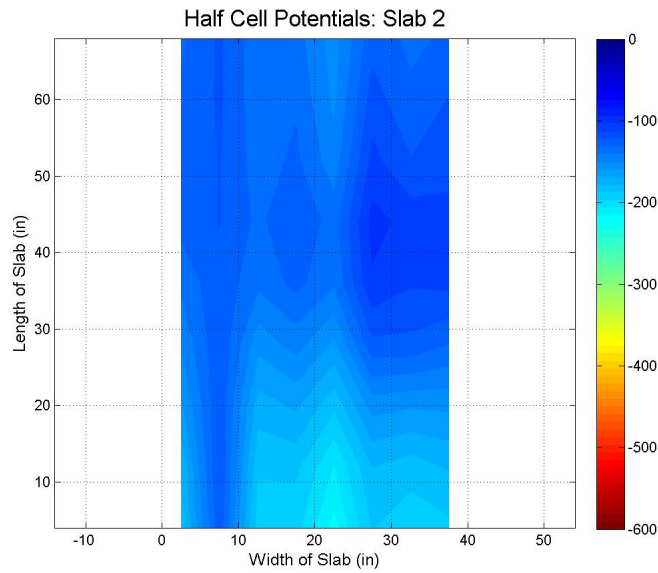


Figure 4.10: Contour Map of Slab 2 on 10 October 2012, Week 40

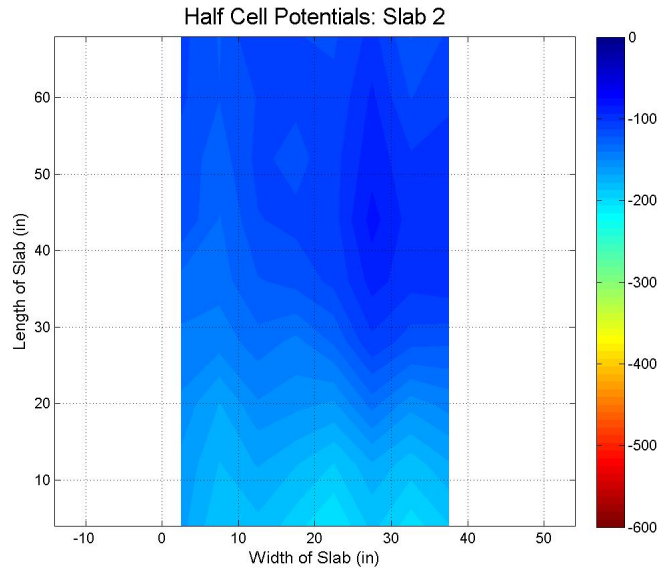


Figure 4.11: Contour Map of Slab 2 on 4 January 2013, Week 52

Slab 2 shows consistent behavior with Slab 1 in that the points of the lowest HCP that occurred at the front of the slab. This is also the farthest point from the voltmeter in the circuit. From this, it is seen that there is a correlation between the magnitude of the HCP and the distance from the voltmeter.

Figure 4.12 shows the curves for the minimum, average, and maximum HCP for the entire test. Curve fitting results using a cubic polynomial for both the minimum and average HCP values are given. The overall HCP graph shows some spikes and dips in the minimum measurements for periods on only one week. These HCP values result in an artificially low  $R^2$  coefficient in the analysis. However, these HCP values were kept because they represent fluctuations that can occur in field applications due to weather, different operators, and similar factors. The average HCP measurements had a much better correlation to Equation (4.1) and are acceptable in this experiment. Table 4.2 contains the parameters for the governing equations.

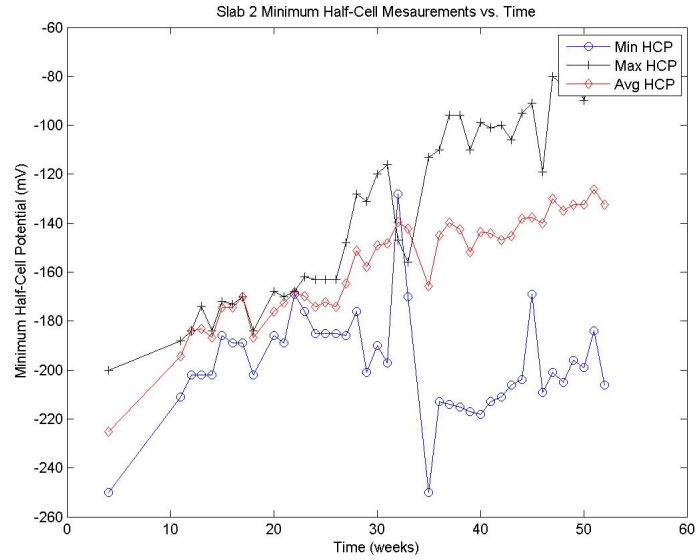


Figure 4.12: Minimum, Average, and Maximum HCP as of Week 52

Table 4.2: Parameters for Slab 2

Measure	P1	P2	P3	P4	R Square
Minimum	.002688	-.2607	7.750	-238.6	.4537
Average	.00089	-.1015	4.971	-237.7	.9064

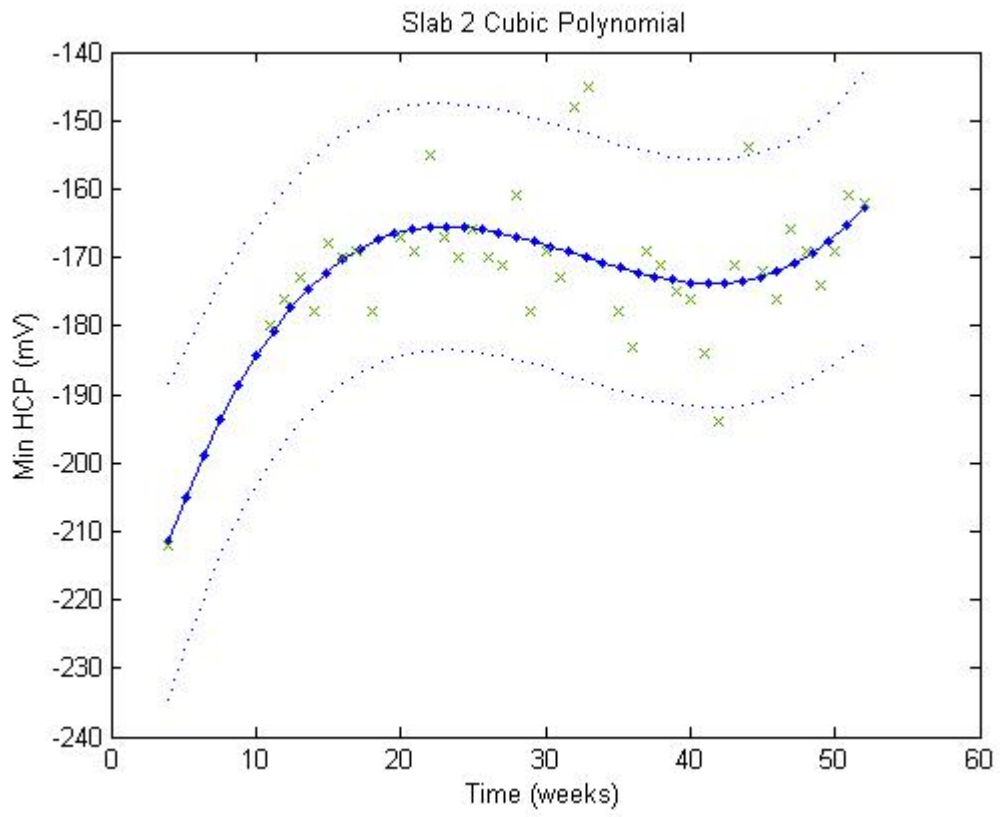


Figure 4.13: Minimum HCP Data and Cubic Polynomial as of Week 52

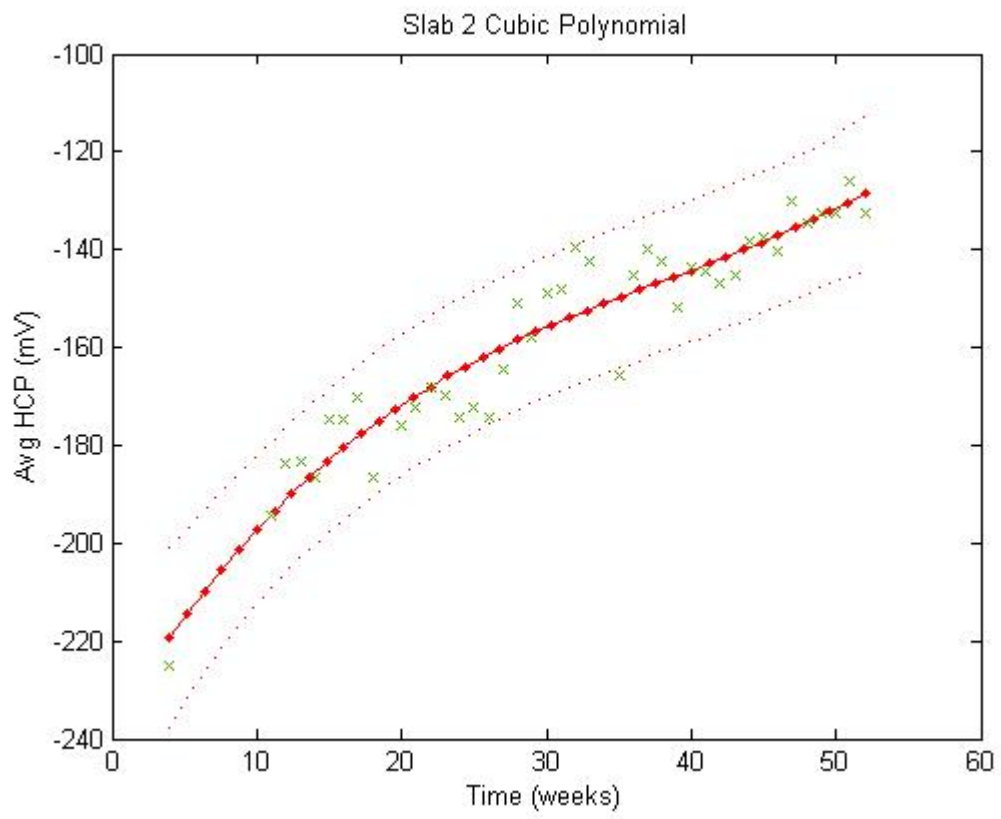


Figure 4.14: Average HCP Data and Cubic Polynomial as of Week 52

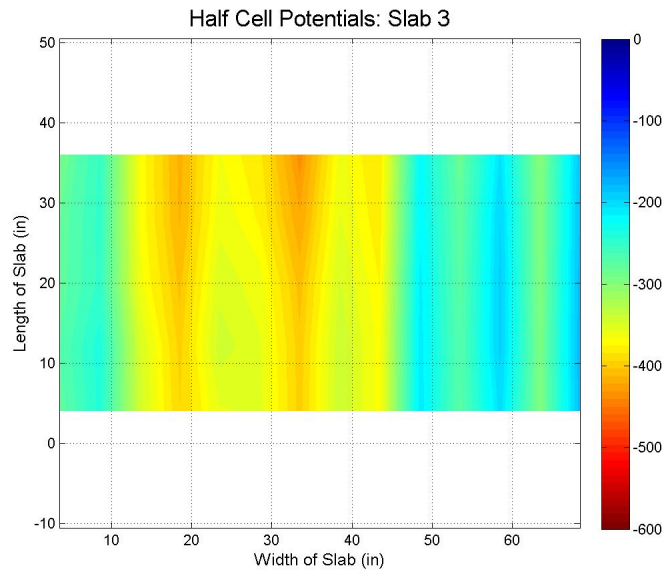


Figure 4.15: Contour Map of Slab 3 on 23 March 2012, Week 11

### 4.1.3 Slab 3

Slab 3 behaved very similarly to Slab 2 in the way that the HCP values stayed relatively consistent. However, unlike Slab 2, there is a large spike in the HCP data of Slab 3 from the start of the experiment until week 10. Again, this is possibly because the concrete was very dry in the first few weeks. After week 15, Slab 3 showed an overall decreasing trend. This is the expected result of the experiment. The starting minimum HCP value was about -500 mV and the final value was about -540 mV predicting that the rebars in Slab 3 are have a greater than 90% probability of being corroded. Figures 4.15 to 19 show the progression of corrosion. Measurements are in millivolts.

The most crucial parameter considered in reaching the result is the concrete cover of the steel rebars. Three separate concrete covers were used in this slab, thus three distinct areas of HCP were expected. However, the HCP contour maps shown in

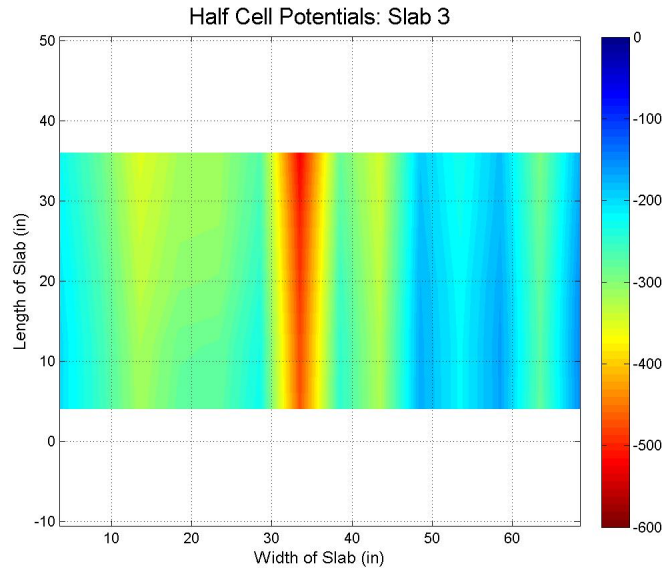


Figure 4.16: Contour Map of Slab 3 on 25 May 2012, Week 20

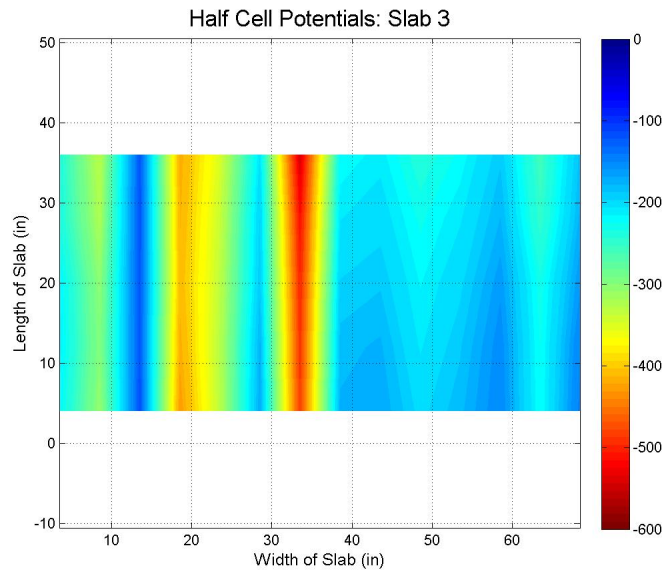


Figure 4.17: Contour Map of Slab 3 on 10 October 2012, Week 40

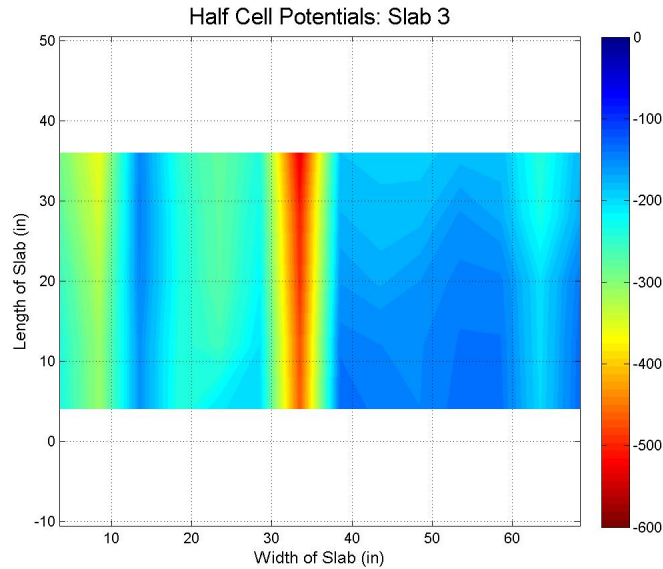


Figure 4.18: Contour Map of Slab 3 on 4 January 2013, Week 52

Figures 4.15 - 18 are clearly not the case. The most likely reason is that the concrete was more penetrable in some areas than in others. Thus, the chlorides were able to reach deeper into the concrete in these areas and active corrosion began in deeper steel rebars before the shallower ones.

Equation (4.1) of Slab 3 reflects the trend, but is not as accurate as the previous two. The early spike in the data throws off the correlation in the minimum HCP analysis. Again, these values were kept in the analysis because they reflect possible variations in field conditions when measurements are taken in field applications.

The average values were much better correlated than the minimum values, but they exhibited an upward trend. The implication is that several points experienced a decrease in HCP, but a larger proportion of points saw an increase. One reason is that the concrete cover varied at different points on the slab. Therefore, while some HCP's decrease, the overall trend is countered by the additional depth of concrete cover for the other rebars. Thus the trend for the average HCP values is reversed. As

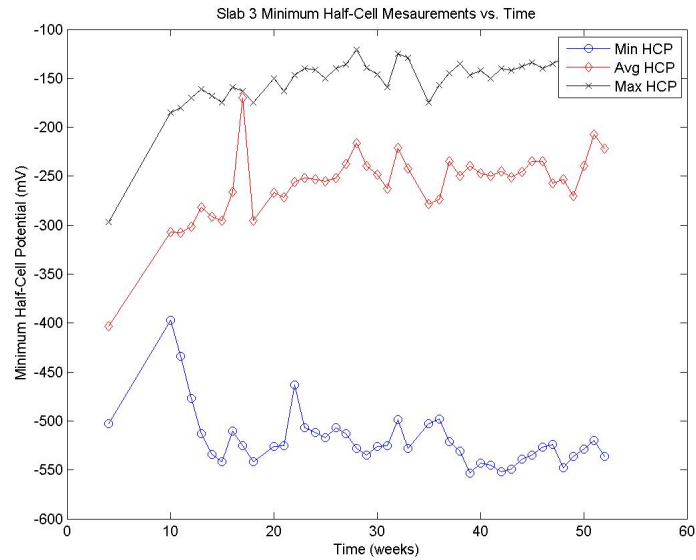


Figure 4.19: Minimum, Average, and Maximum HCP as of Week 52

Table 4.3: Parameters for Slab 3

Measure	P1	P2	P3	P4	R Square
Minimum	$-5.64 \times 10^{-6}$	.03406	-3.235	-457.0	.3132
Average	$6.58 \times 10^{-3}$	-.6689	21.77	-473.8	.6618

in the previous sections, the maximum HCP was only plotted for reference and the parameters for the governing equation are given in the Table 4.3.

#### 4.1.4 Slab 4

Slab 4 is the control slab; it has not been ponded since the beginning of the experiment. As such, the HCP remained high throughout the entire experiment. Visual inspection showed no corrosion on the surface of the slab. The rebar configuration is the same as Slab 3. The minimum HCP remained steady until Week 30 when the

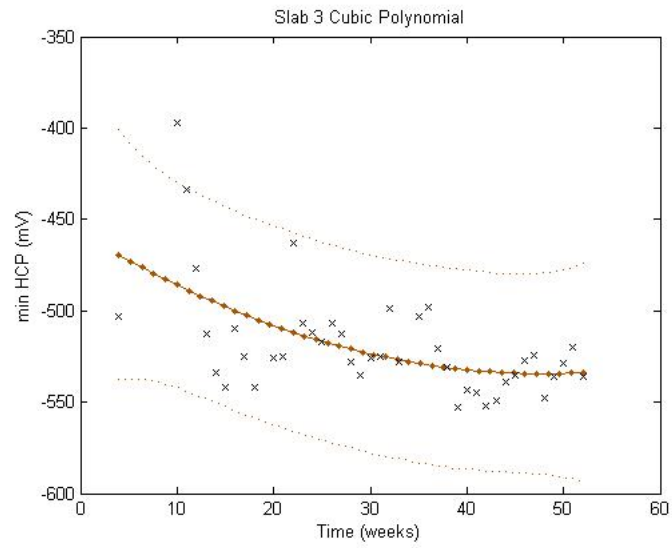


Figure 4.20: Minimum HCP Data and Cubic Polynomial as of Week 52

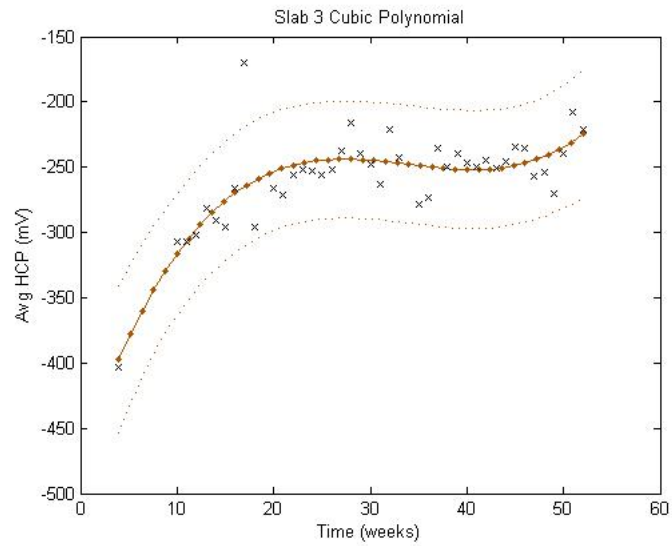


Figure 4.21: Average HCP Data and Cubic Polynomial as of Week 52

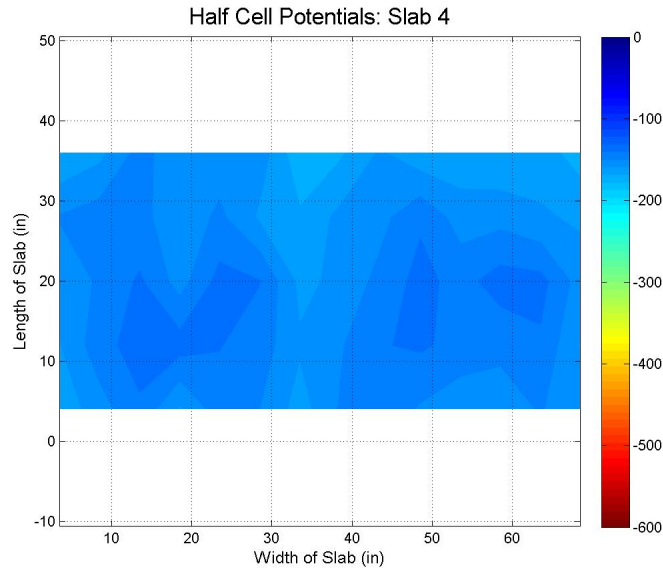


Figure 4.22: Contour Map of Slab 4 on 23 March 2012, Week 11

values suddenly dipped and then fluctuated as much as 150 mV in either direction in two weeks. The most likely reason is that these HCP measurements indicate noise in the data. The data would have to be smoothed out in order to increase the accuracy of the measurements. The HCP was about -180 mV at the start of the experiment and varied between -170 mV and -50 mV after week 30. Figures 4.22 to 25 show the HCP of the control specimen. Measurements are in millivolts.

The spontaneity in the HCP measurements on Slab 4 (see Figure 4.26) makes the analysis less accurate because the measurements are more spread out. However, the trend in both the average and the minimum HCP is increasing overall. The volatility in HCP was not confined to a specific area, but was spread out over the entire slab. Thus, the average HCP has only a slightly better correlation. Still, both model curves accurately fit the data and can be used to predict the amount of noise in the data after years of field testing. The curves and parameters are given in Table 4.4.

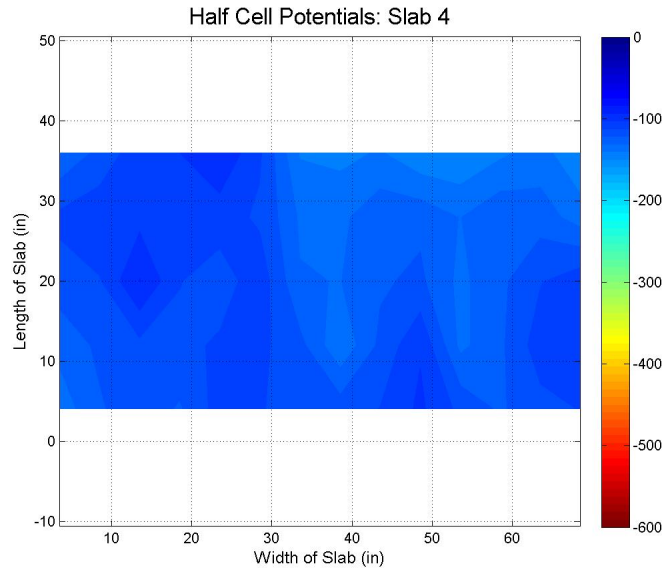


Figure 4.23: Contour Map of Slab 4 on 25 May 2012, Week 20

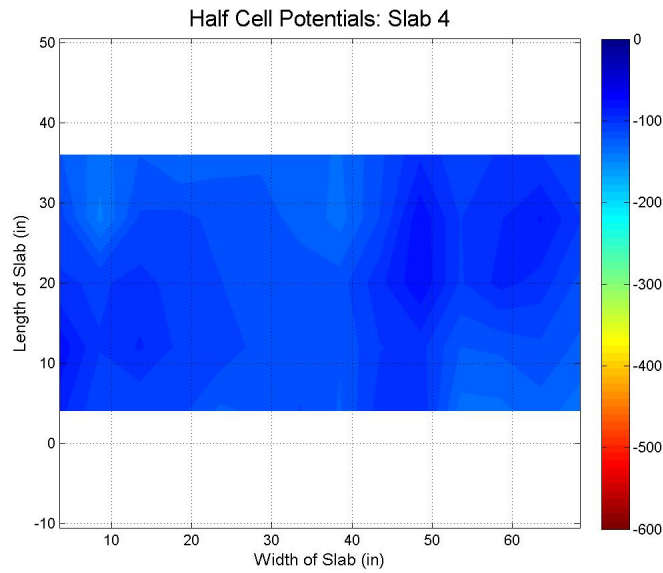


Figure 4.24: Contour Map of Slab 4 on 10 October 2012, Week 40

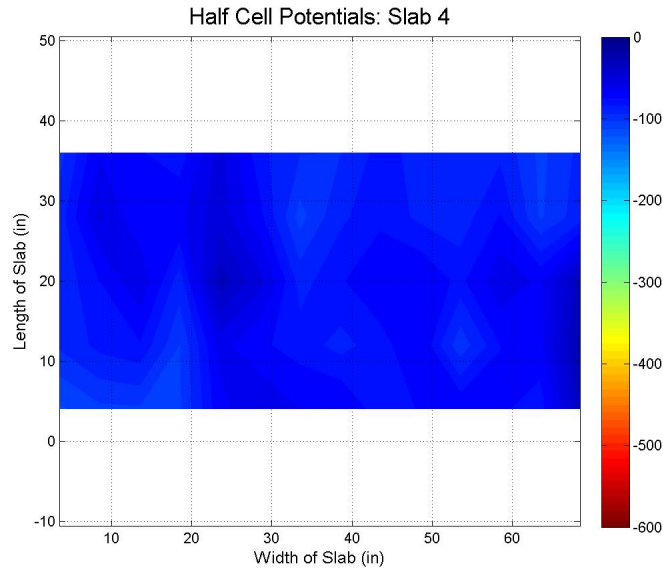


Figure 4.25: Contour Map of Slab 4 on 4 January 2013, Week 52

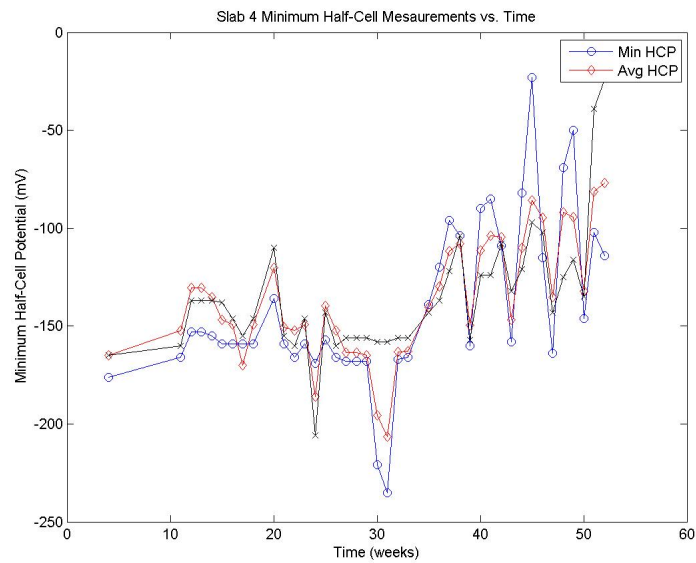


Figure 4.26: Minimum, Average, and Maximum HCP as of Week 52

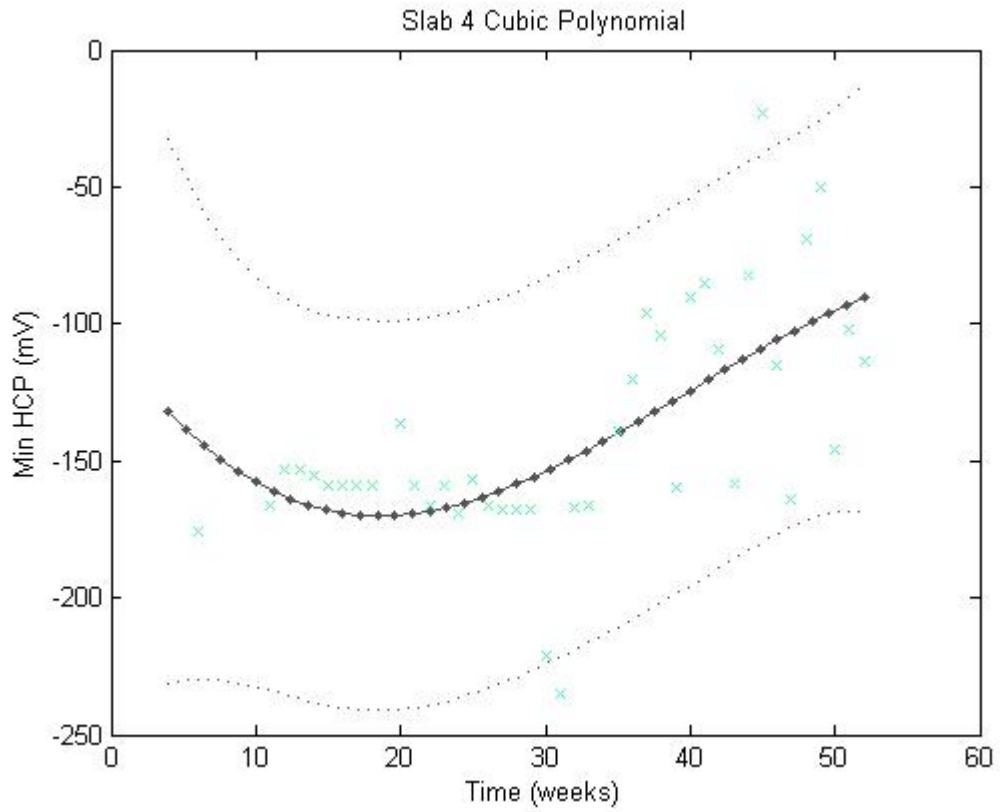


Figure 4.27: Minimum HCP Data and Cubic Polynomial as of Week 52

Table 4.4: Parameters for Slab 4

Measure	P1	P2	P3	P4	R Square
Minimum	-.00231	.2762	-7.857	-104.6	.4030
Average	.000542	.03798	-2.601	-123.2	.5263

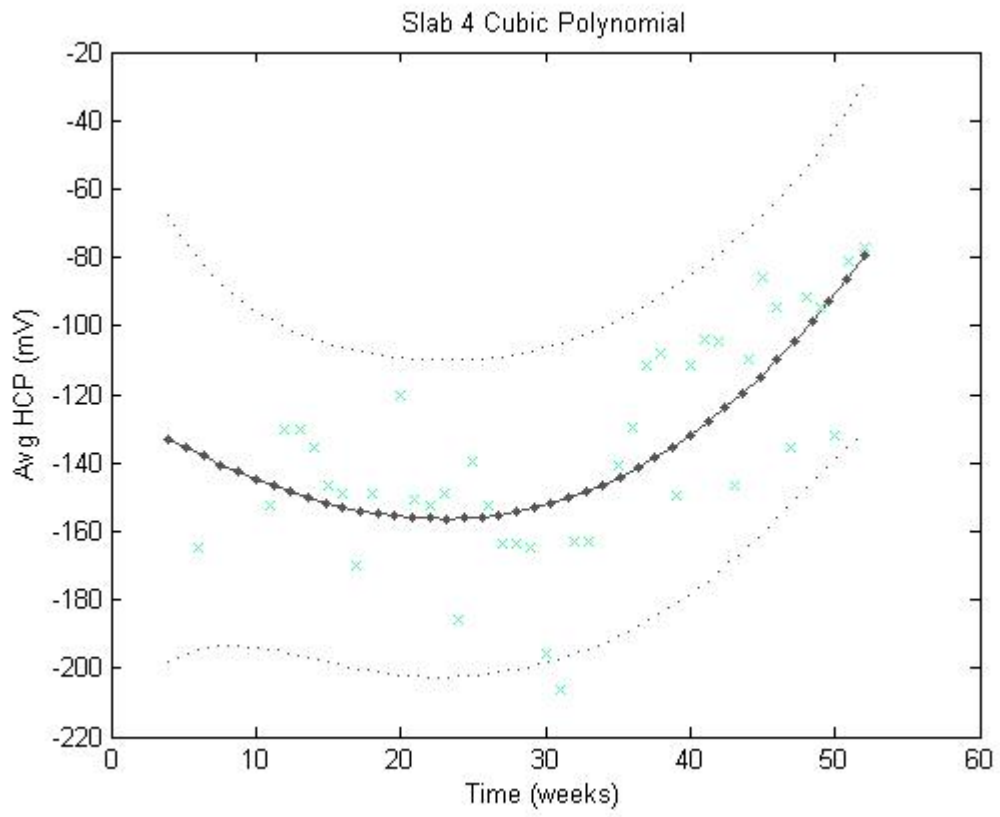


Figure 4.28: Average HCP Data and Cubic Polynomial as of Week 52

## 4.2 Current Density

The reason for relating current density to HCP is simple. To take measurements, a current must be induced in the rebars. The current will remain the same over the relatively short circuit in the test setup. The size of the rebars and wires is sufficiently large, and the circuit short enough, to make voltage drop negligible in the parts of the circuit not under investigation. Thus, the only factor that causes any change in the circuit is the size of the rebar. Rebar diameter decreases as corrosion occurs and controls the current density. As the rebar diameter decreases, the same amount of current must travel through the same rebar. Therefore, the current density increases the most in the bars with the greatest corrosion. However, our experiment showed that the current density is much more variable than expected. Current density was not measured, but was calculated by Equation (2.2).

The data was compared to the results in Reou and Ann (2009). There was no quantitative correlation between their data and the data in this research, however qualitative comparisons could be made. The following subsections discuss each slab in more detail.

### 4.2.1 Slab 1

As expected, the rebars in Slab 1 exhibit increasing current densities with time indicating the notion relating HCP to current density is correct. However, the increase is an overall trend not reflected in the weekly measurements. Also, all of the data from different rebars in the slab tends to follow each other throughout the experiment indicating that the rebars have a good correlation to each other. The variability in the measurements can not be attributed to changes in HCP because the data does not coincide. That is, the increases and decreases in the current density are not in

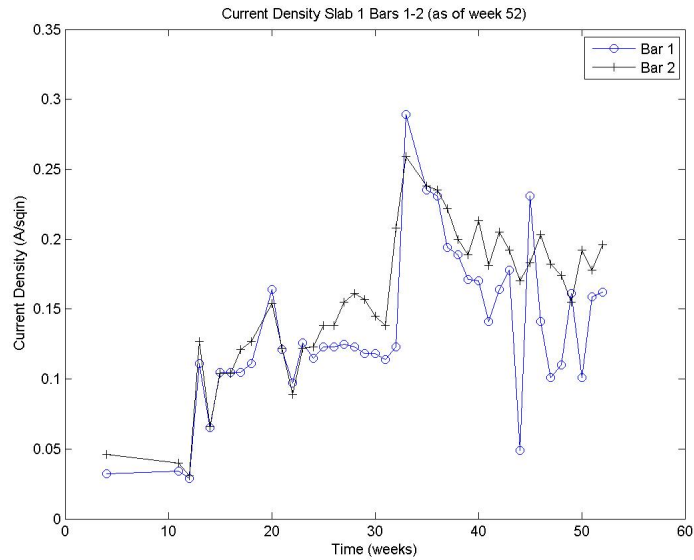


Figure 4.29: Current Density of Slab 1, Bars 1 and 2

agreement with the increases and decreases in weekly HCP readings. Figures 4.29 to 4.33 show the results of the current density calculations.

Comparing the current densities from Week 4 to Week 52, all of the rebars except for one increased. Rebar 7 did not increase as expected, but held relatively steady throughout the experiment. Overall, the current density increased significantly, showing a  $0.08 \text{ A/in}^2$  (165%) rise in the fifty-two weeks. The Table 4.5 contains the current density in Weeks 4 and 52 and both the absolute and percent changes in current density for each rebar. Absolute change is measured in  $\text{A/in}^2$ .

### 4.2.2 Slab 2

Slab 2 also had very good correlation between the current density measurements of the individual bars. But unlike Slab 1, the increases of the current density were much greater both in the absolute measure and the percent increase. This is counterintuitive because Slab 2 has an additional half-inch of cover. Furthermore, no visual evidence

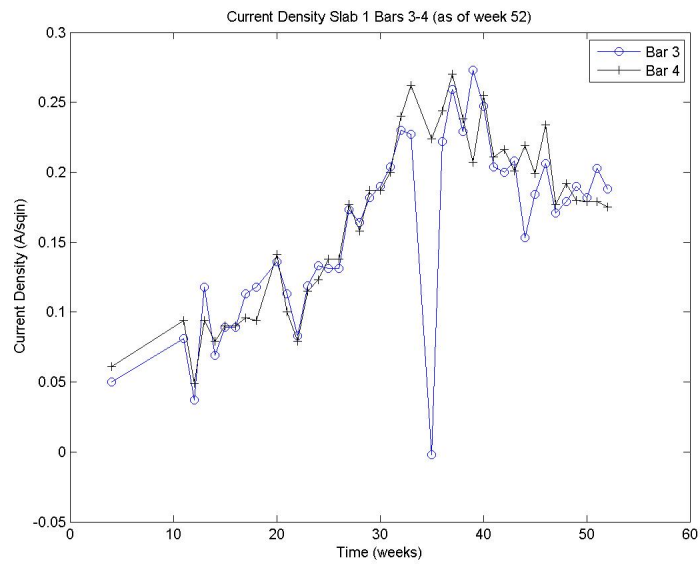


Figure 4.30: Current Density of Slab 1, Bars 3 and 4

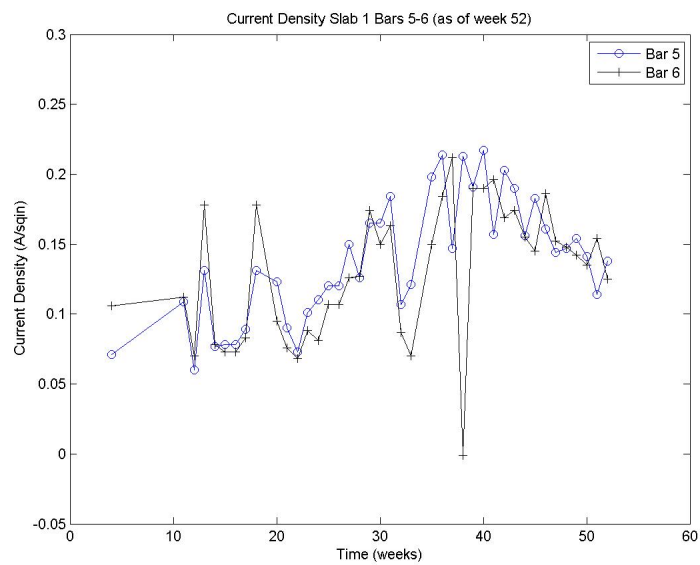


Figure 4.31: Current Density of Slab 1, Bars 5 and 6

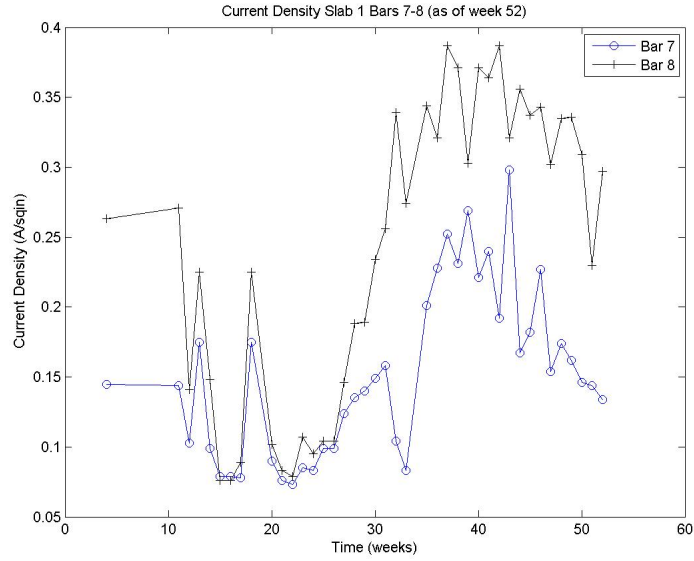


Figure 4.32: Current Density of Slab 1, Bars 7 and 8

Table 4.5: Current Densities and Changes for Slab 1

Bar Number	1	2	3	4	5	6	7	8
Week 4	0.032	0.046	0.050	0.061	0.071	0.106	0.145	0.263
Week 52	0.162	0.196	0.188	0.175	0.138	0.125	0.134	0.297
Absolute Change	0.130	0.151	0.138	0.115	0.066	0.019	-0.011	0.034
Percent Change	408	332	278	189	93	18	-8	13

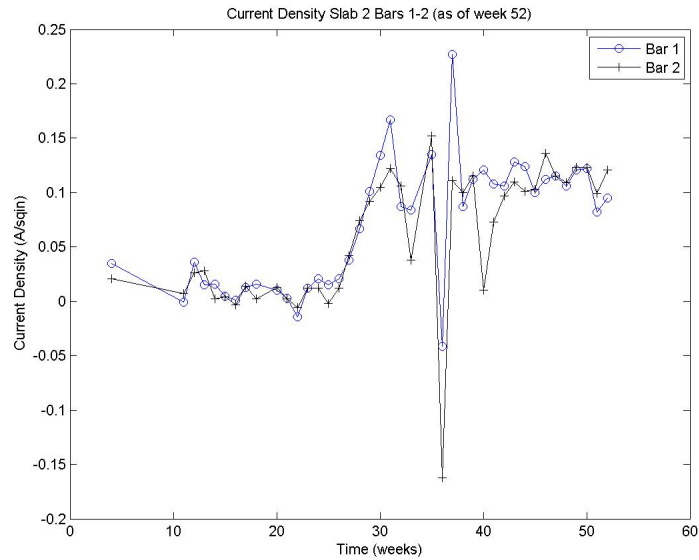


Figure 4.33: Current Density of Slab 2, Bars 1 and 2

exists on the surface of Slab 2 to confirm the presence of active corrosion. The most likely reason for the increase in current density is that the current has no easy path to complete the circuit. It is possible that the ends of the wires used to connect the voltmeter to the bars are corroded to such an extent that the current can not use the entire connection to travel to the rebars from the voltmeter. Figures 4.33 - 37 show the current densities in each rebar and Table 4.6 gives the absolute and percent increases. The average absolute increase was  $0.165 \text{ A/in}^2$  and the average percent increase was 1136%. Measurements are in millivolts.

### 4.2.3 Slab 3

Like Slab 2, the rebars in Slab 3 all show similar trends. However, the weekly changes and the start-to-end change were much less dramatic than Slab 2. Furthermore, a distinct difference exists between the first five rebars and the other nine rebars. Rebars 1-5 all have 1.5" cover whereas rebars 6-10 have 2" cover and rebars 11-14 have 2.5" of

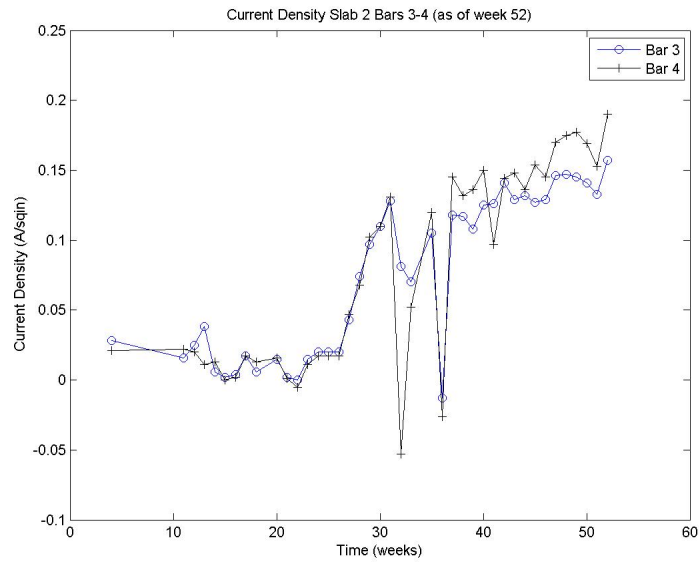


Figure 4.34: Current Density of Slab 2, Bars 3 and 4

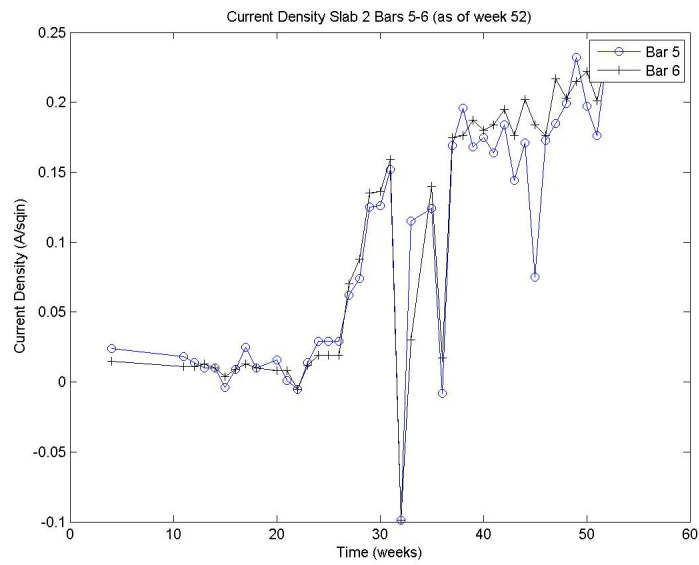


Figure 4.35: Current Density of Slab 2, Bars 5 and 6

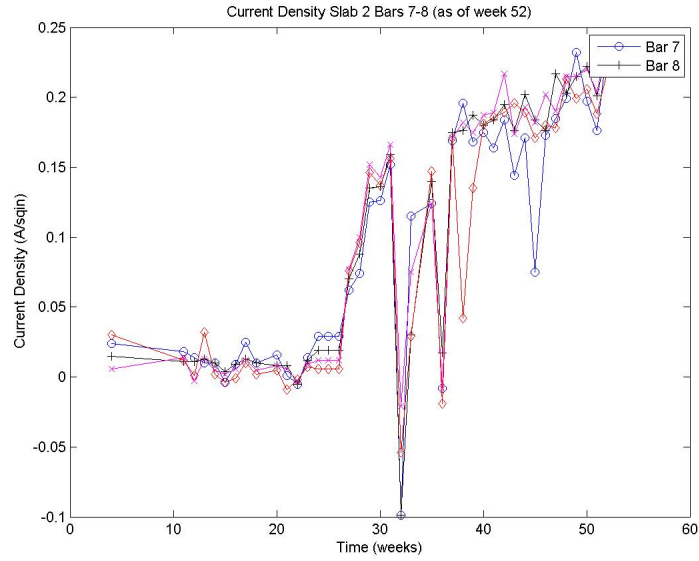


Figure 4.36: Current Density of Slab 2, Bars 7 and 8

Table 4.6: Current Densities and Changes for Slab 2

Bar Number	1	2	3	4	5	6	7	8
Week 4	0.035	0.021	0.028	0.021	0.024	0.015	0.006	0.030
Week 52	0.095	0.121	0.157	0.190	0.238	0.236	0.240	0.219
Absolute Change	0.060	0.101	0.128	0.168	0.214	0.222	0.235	0.188
Percent Change	173	486	452	795	905	1515	4138	623

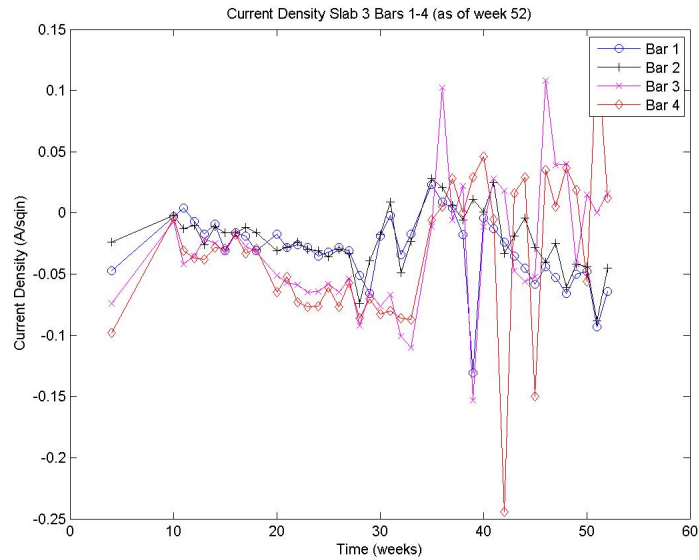


Figure 4.37: Current Density of Slab 3, Bars 1 - 4

cover. This implies that concrete cover is an influencing factor in the current density calculations; the change in current density is greatest where the cover is the least. At this time, the exact relationship between concrete cover and current density is unknown, but after a depth of two inches, the effect is muted. For instance, Rebar 5 exhibited a 137% change from Week 4 to Week 52 vs. a maximum change of 50% for the other nine. Figures 4.37 to 4.40 show the current densities in each rebar with time and Table 4.7 shows the current densities at the beginning and the end of the test measured in  $A/in^2$ , along with the absolute and percent changes. The average absolute change was  $-0.019 A/in^2$  and the average percent change was 18%. The current density values are listed in rows two through four of Table 4.7 are the opposite of the actual data. This occurred because of the reference system used to calculate the current density. The values for the percent change is correct. The data and absolute change is in  $mA/in^2$ .

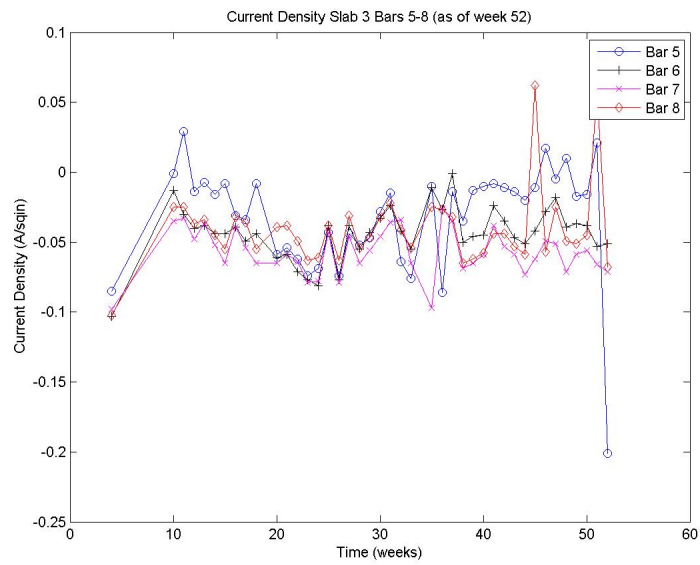


Figure 4.38: Current Density of Slab 3, Bars 5 - 8

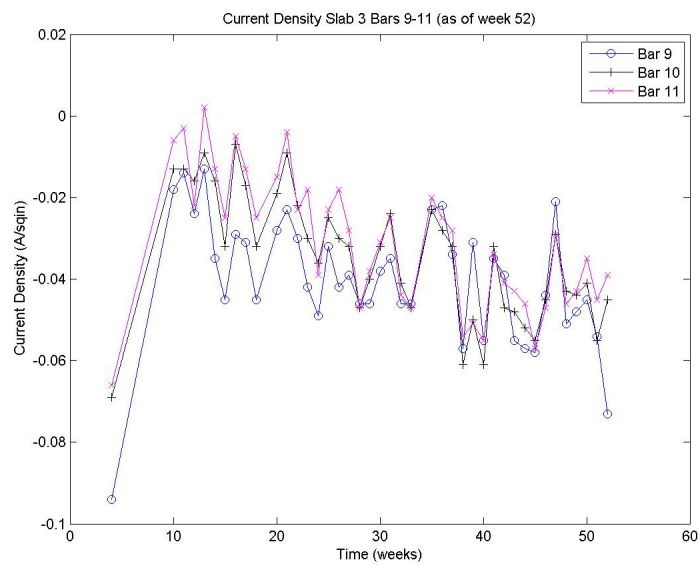


Figure 4.39: Current Density of Slab 3, Bars 9 - 11

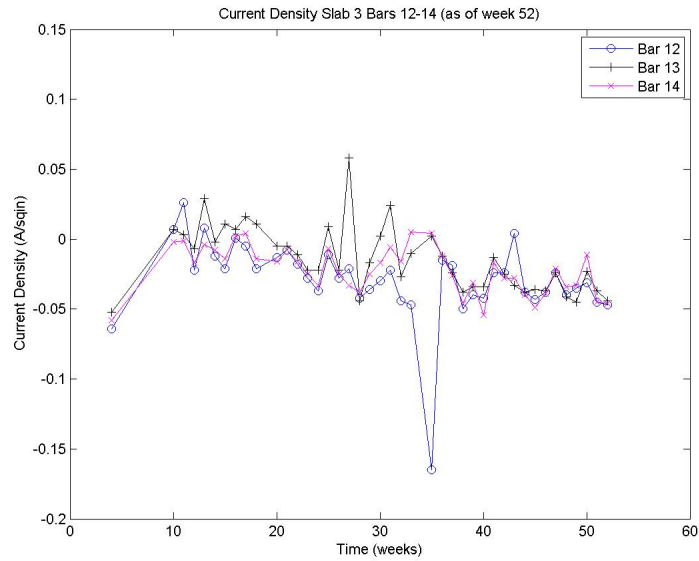


Figure 4.40: Current Density of Slab 3, Bars 12 - 14

Table 4.7: Current Densities and Changes for Slab 3

Bar Number	1	2	3	4	5	6	7
Week 4	-47	-24	-74	-98	-85	-103	-98
Week 52	-64	-45	16	12	-201	-51	-71
Absolute Change	17	21	-90	-110	117	-52	-27
Percent Change	-36	-85	121	112	-137	50	27
Bar Number	8	9	10	11	12	13	14
Week 4	-102	-94	-69	-66	-64	-52	-58
Week 52	-68	-73	-45	-39	-47	-44	-46
Absolute Change	-34	-21	-23	-27	-17	-8	-13
Percent Change	34	23	34	41	26	16	22

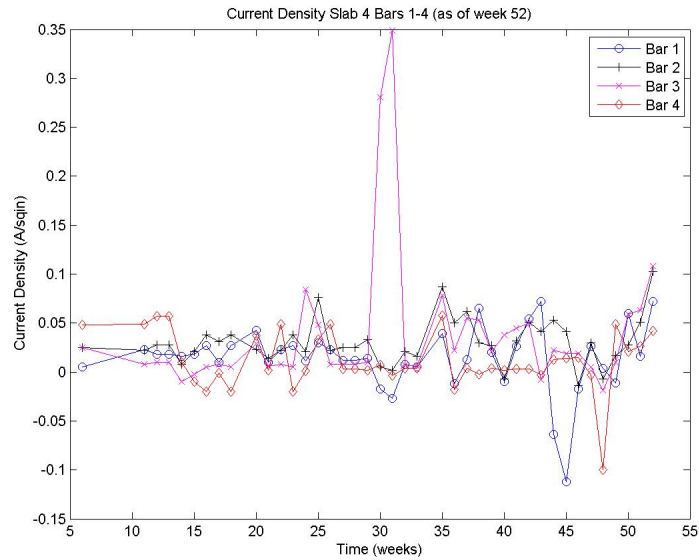


Figure 4.41: Current Density of Slab 4, Bars 1 - 4

#### 4.2.4 Slab 4

Slab 4 also shows the trend that the current density in each rebar followed a similar pattern. The notable exception is the data of the first five bars. (1.5” concrete cover). This provides further evidence that the concrete cover is an important factor in the current density calculations. Although Slab 4 was the control, there is no numerical pattern to the current density changes throughout the slab. This is an indicator of noise in the measurements that should be removed for a more detailed analysis. Figures 4.41 through 4.44 show the current density throughout the experiment. Table 4.8 provides the initial and final values of the current density in mA/in<sup>2</sup> and the absolute and percent changes. The average absolute change was 13 mA/in<sup>2</sup> and the average percent change was 250%.

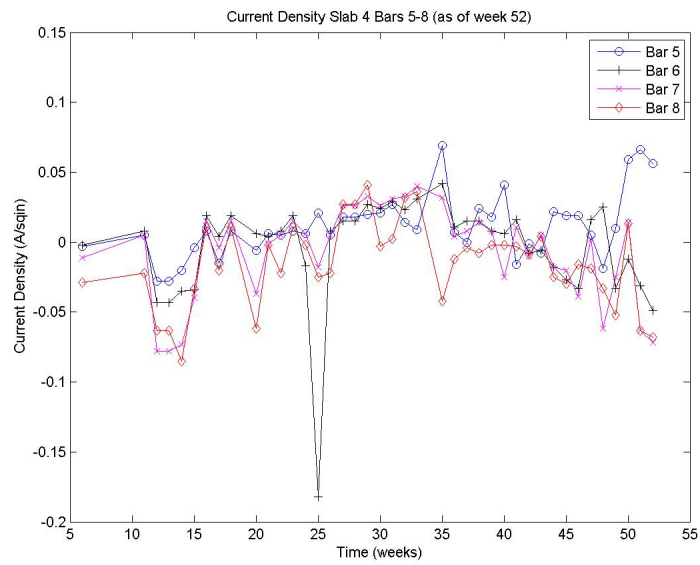


Figure 4.42: Current Density of Slab 4, Bars 5 - 8

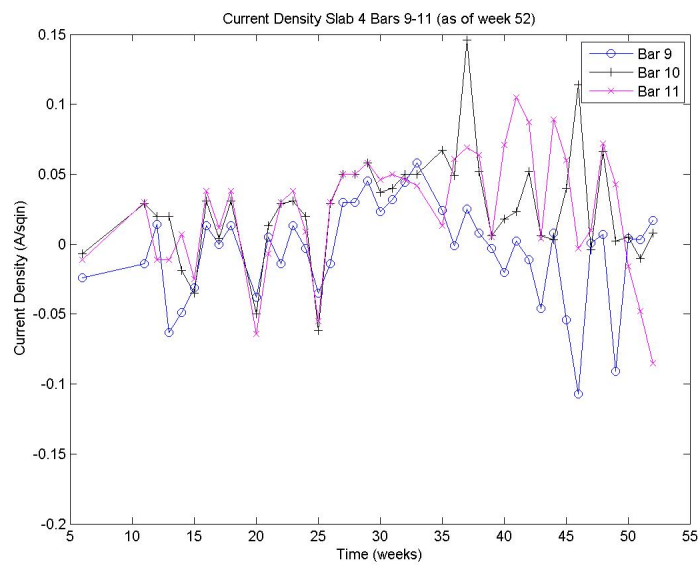


Figure 4.43: Current Density of Slab 4, Bars 9 - 11

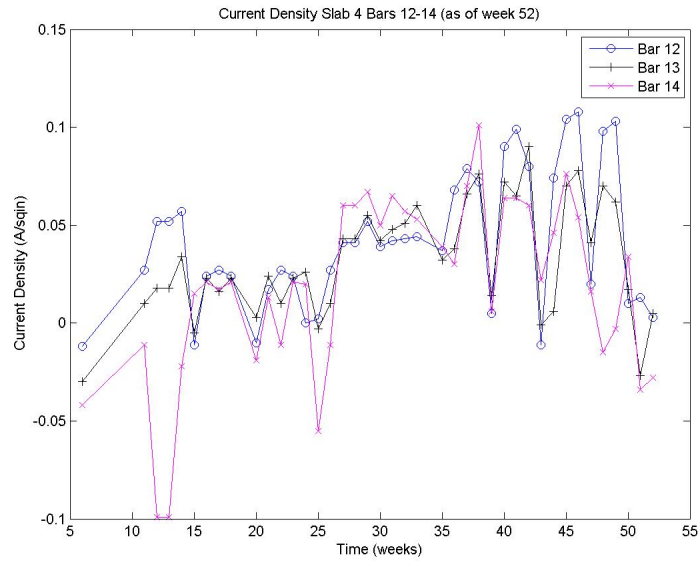


Figure 4.44: Current Density of Slab 4, Bars 12 - 14

Table 4.8: Current Dneisties and Changes for Slab 4

Bar Number	1	2	3	4	5	6	7
Week 4	5	25	25	48	.3	-2	-11
Week 52	72	103	108	42	56	-49	-72
Absolute Change	67	78	83	-6	59	-47	-61
Percent Change	1318	309	336	-13	-1754	2579	552
Bar Number	8	9	10	11	12	13	14
Week 4	-29	-24	-7	-11	-12	-30	-42
Week 52	-68	17	8	-85	3	5	-28
Absolute Change	-39	41	16	74	15	36	13
Percent Change	134	-169	-211	693	-125	-117	-32

## 4.3 Summary

This chapter discusses the trends observed in the HCP of each slab and discusses the plotting of the minimum and average HCP. Curve fitting was examined; a cubic polynomial was developed to best represent the HCP data. The concrete cover was found to be the most important factor influencing the rate of corrosion as corrosion was only observed on Slab 1. Parameters for the polynomial equations are given in Tables 4.1 - 4 in Section 4.1.

In Section 4.2, the current density in each bar was also discussed and plotted against the time of the experiment. Trends in how the data changed over time were discussed and explained. The influence of concrete cover on current density was also observed in this section. Relevant information can be found in Tables 4.5 - 8 in Section 4.2.

# Chapter 5

## Conclusions

In this thesis, the HCP data of four reinforced concrete slabs was collected and analyzed. Three of the slabs were ponded in weekly cycles using a slightly altered version of the Modified Southern Exposure Test. The data was collected at several points along each rebar. The HCP data from each rebar was then compared to the other rebars in the same slab. Slabs 1,2, and 3 were also compared to each other and to the control slab, Slab 4. Trends in the HCP data were analyzed. Curve fitting was performed to determine the best model for the HCP data.

Additionally, the current density was calculated using Eq. (2.2) and compared to existing research to verify the trends in the data presented herein. The current density data of individual rebars was plotted in the time domain and qualitatively related to other rebars and other slabs. Similar trends were observed in three of the slabs. Possible reasons for the data projections were given. Changes in the data were quantified by both absolute and percent change from the start of the test to the end of the recorded HCP data.

## 5.1 Research Findings

- Spatial Distribution of HCP

HCP decreases with distance from the voltmeter. Each slab contained rebars with either nine or fourteen measurements taken on each rebar. The effect was most noticeable on longer bars because the distance between the voltmeter and the point of measurement was greater. HCP was also lower on the edges of slabs than in the center, provided that the rebars all had the same concrete cover. Consequently, the highest HCP on any slab will be observed in the middle at the point closest to the connection to the voltmeter.

Modeling the HCP was done accurately with cubic polynomials using the  $R^2$  as an indicator of correlation. Results indicated that the average HCP could be modeled more accurately than the minimum HCP values and should be used in predicting future HCP values.

- Effect of Concrete Cover on HCP

Concrete cover is the most important factor in the measured HCP. The most effective comparison was between Slabs 1 and 2. Slab 1 had 1.5" of cover, Slab 2 had 2" of cover. This small difference significantly i) increased the time for chlorides to penetrate the concrete cover and ii) increased the time to the breakdown of the passive layer on steel rebars.

- Current Density

Current density is significantly affected by the amount of concrete cover over the rebars. Rebars with more than 1.5" cover all showed similar trends when individual rebars were compared to each other. However, rebars with 1.5" cover were much more sporadic when compared to other rebars in the same slab. This

is because the chlorides attacked the passive layer and began active corrosion on the rebars with less cover sooner than the rebars with more cover. In each slab, the current densities rose when analyzed in the time domain. This agreed with current literature and intuition.

## 5.2 Contributions

- HCP is decreases with distance from the voltmeter
- Time domain HCP data can be accurately modeled using cubic polynomials
- Current density data becomes more sporadic as active corrosion advances in steel rebars

## 5.3 Future Work

This thesis contains research work on reinforced concrete slabs with steel rebars electrically separated from each other by five inches of concrete on either side. To better model existing structures, the rebars should be connected electrically with longitudinal and transverse reinforcing. Furthermore, the surface crack patterns should be analyzed to determine the relationship between crack patterns and the level of reinforcing. This will provide a much simpler indication of the amount of corrosion present in the reinforcement. HCP models may also be revised to derive a simpler equation for the HCP in the time domain. Also, based on the HCP data from Slab 4, the environmental noise may be removed from the HCP measurements to more accurately model the data.

The current density can also be analyzed and modeled by empirical relationships

between the rebars and time. Such analysis will allow the prediction of future current density values and, as this is currently not well understood, improvements in the analysis will be invaluable to future research. Moreover, the relation between the current density and the HCP could be further refined to obtain the most accurate relationship available.

# References

1. Batis, G., Kouloumbi, N., and Kotsakou, K. (1997). "Corrosion and Protection of Carbon Steel in Low Enthalpy Geothermal Fluids. The Case of Sousaki in Greece." *Geothermics*, 26(1). 65-82.
2. Cabrera, J. G. (1997). "Deterioration of Concrete Due to Reinforcement Steel Corrosion." *Cement & Concrete Composites*, 18. 47-59.
3. Castro, P., Veleva, L., and Balanca, M. (1997). "Corrosion of Reinforced Concrete in a Tropical Marine Environment." *Construction and Building Materials*, 11(2). 75-81
4. Darwin, D., Balma, J., Locke Jr., C. E., and Nguyen, T. V. (2001). "Accelerated testing for Concrete Reinforcing Bar Corrosion Protection Systems." *Long Term Durability of Structural Materials*, 97-108.
5. Duffo, G. S., Arva, E. A., Schulz, F. M., and Vazquez, D. R. (2012). "Evaluation of the Corrosion of a Reinforced Concrete Designed For the Construction of an Intermediate-level Radioactive Waste Disposal Facility." *Procedia Materials Science*, 1. 215-221.
6. Duong, V. B., Sahamitmongkol, R., and Tangtermsirikul, S. (2013). "Effect of Leaching on Carbonation Resistance and Steel Corrosion of Cement-Based

- Materials." *Construction and Building Materials*, 40. 1066-1075.
7. Elsener, B. (2001). "Half-Cell Potential Mapping to Assess Repair Work on RC Structures." *Construction and Building Materials*, 15. 133-139.
  8. Frolund, T., Klinghoffer, O., and Sorensen, H. E. (July 2003). "Pros and Cons of Half-Cell Potential and Corrosion Rate Measurements." Structural Faults and Repairs, International Conference, London, U.K. 1-11.
  9. Gonzalez, J. A., Miranda, J. M., Feliu, S. (2004). "Considerations on Reproducibility of Potential and Corrosion Rate Measurements in Reinforced Concrete." *Corrosion Science* 46. 24678-2485.
  10. Gulikers, J. J. W. (2009). Application of a Statistical Procedure to evaluate the Results from Potential Mapping on a Parking Garage." *Taylor and Francis Group*, 267-273.
  11. Guzman, S., Galvez, J. C., and Sancho, J. M. (2011). "Cover Cracking of Reinforced Concrete Due to Rebar Corrosion Induced by Chloride Penetration." *Cement and Concrete Research*, 41. 893-902.
  12. Hussain, R. R. (2011). "Underwater Half-Cell Corrosion Potential Bench Mark Measurements of Corroding Steel in Concrete Influenced by a Variety of Material Science and Environmental Engineering Variables." *Measurement*, 274-280.
  13. Kranc, S. C. and Sagues, A. A. (2001). "Detailed Modeling of Corrosion Macro-cells on Steel Reinforcing in Concrete." *Corrosion Science*, 1355-1372.
  14. LNEC. (May 2012). "Electrical and Electrochemical Techniques: Concrete Resistivity Half-Cell Potential Corrosion Rate." ENEC, Lisbon, Portugal

15. Leerlalerkiet, V., Kyung, J-W., Ohtsu, M., and Yokota, M. (2004). "Analysis of half-Cell Potential Measurement for Corrosion of Reinforced Concrete." *Construction and building materials*, 18. 155-162.
16. Li, C. Q. (July-August 2001). "Initiation of Chloride-Induced Reinforcement Corrosion in Concrete Structural Members - Experimentation." *ACI Structural Journal*, 502-510.
17. Li, C. Q. and Melchers, R. E. (September-October 2005). "Time-Dependent Risk Assessment of Structural Deterioration Caused by Reinforcement Corrosion." *ACI Structural Journal*, 754-761.
18. Lu, C., Jin, W, and Liu, R. (2011). "Reinforcement Corrosion-Induced Cover Cracking and its Time Prediction for Reinforced Concrete Structures." *Corrosion Science*, 53. 1337-1347.
19. Maruya, T., Takeda, H., Horiguchi, K., Koyama, S., Hsu, K-L. (2007). "Simulation of Steel Corrosion in Concrete Based on the Model of Macro-Cell Corrosion Circuit." *Journal of Advanced Concrete Technology*, 5(3). 343-362.
20. Muralidaran, S., Saraswathy, V., Madhavamayandi, A., Thangavel, K., and Palaniswamy, N. (2008). "Evaluation of Embeddable Potential Sensor for Corrosion monitoring in Concrete Structures." *Electrochimica Acta*, 7548-7254.
21. Ohtsu, M. and Yamamoto, T. (1997). "Compensation Procedure for Half-Cell Potential Measurement." *Construction and Building Materials*, 11(7-8). 395-402.
22. Otieno, M. B., Alexander, M. G., and Beushausen, H. D. (September-October 2010). "Suitability of Various Measurement Techniques for Assessing Corrosion

- in Cracked Concrete.” *ACI Structural Journal*, 481-489.
23. Pech-Canul, M. A. and Castro, P. (2002). ”Corrosion Measurements of Steel Reinforcement in Concrete Exposed to a Tropical Marine Atmosphere.” *Cement and Concrete Research*, 32. 491-498.
  24. Poupard, O., L’Hostis, V., Catinaud, S., and Petre-Lazar, I. (2006). ”Corrosion Damage Diagnosis of a Reinforced Concrete Beam After 40 Years Natural Exposure in Marine Environment.” *Cement and Concrete Research*, 504-520.
  25. Pradhan, B. and Bhattacharjee, B. (2011). ”Rebar Corrosion in Chloride Environment.” *Construction and Building Materials*, 25. 2565-2575.
  26. Reou, R. S. and Ann, K. Y. (2009). ”Electrochemical Assessment of the Corrosion Risk of Steel Embedment in OPC Concrete Depending on the Corrosion Detection Techniques.” *Materials Chemistry and Physics* 113. 78-84
  27. Sadowski, L. (2010). ”New Non-Destructive Method for Linear Polarisation Resistance Corrosion Rate Measurement.” *Archives of Civil and Mechanical Engineering*, X(2).
  28. Topcu, I. B., Boga, A. R., and Hocaoglu, F. O. (2009). ”Modeling Corrosion Currents of Reinforced Concrete Using ANN.” *Automation in Construction*, 18. 145-152.
  29. Trejo, D. and Pillai, R. G. (November-December 2003). ”Accelerated Chloride Threshold Testing: Part I - ASTM A615 and A706 Reinforcement.” *ACI Structural Journal*, 519-527.
  30. Trejo, D. and Pillai, R. G. (January-February 2004). ”Accelerated Chloride

- Threshold Testing - Part II: Corrosion-Resistant Reinforcement." *ACI Structural Journal*, 57-64.
31. Yuan, Y., Ji, Y., and Shah, S. P. (May-June 2007). "Comparison of Two Accelerated Corrosion Techniques for Concrete Structures." *ACI Structural Journal*, 344-347.
  32. Yuzer, N., Akoz, F., and Kabay, N. (2008). "Prediction of Time to Crack Initiation in Reinforced Concrete Exposed to Chloride." *Construction and Building Materials*, 22. 1100-1107.
  33. Zhang, J., Monteiro, P. J. M., and Morrison, H. F. (2001). "Experimental and Theoretical Study of Reinforced Concrete Corrosion Using Impedance Measurements." *Long Term Durability of Structural Materials*, 71-84.